npj | biofilms and microbiomes

Article

Published in partnership with Nanyang Technological University

https://doi.org/10.1038/s41522-024-00593-7

Combating biofilm-associated *Klebsiella pneumoniae* infections using a bovine microbial enzyme

Reshma Ramakrishnan[1], Abhilash V. Nair[2], Kirti Parmar[2], Raju S. Rajmani[3], Dipshikha Chakravortty[2,4] ✉ & Debasis Das[1] ✉

The emergence of multidrug-resistant *Klebsiella pneumoniae* poses significant clinical challenges with limited treatment options. Biofilm is an important virulence factor of *K. pneumoniae*, serving as a protective barrier against antibiotics and the immune system. Here, we present the remarkable ability of a bovine microbial enzyme to prevent biofilm formation (IC_{50} 2.50 μM) and degrade pre-formed *K. pneumoniae* biofilms (EC_{50} 1.94 μM) by degrading the matrix polysaccharides. The treatment was effective against four different clinical *K. pneumoniae* isolates tested. Moreover, the enzyme significantly improved the biofilm sensitivity of a poorly performing broad-spectrum antibiotic, meropenem, and immune cells, resulting in facile biofilm clearance from the mouse wound infection. Notably, well-known powerful enzymes of the same class, cellulase, and α-amylase, were nearly inactive against the *K. pneumoniae* biofilms. The enzyme exhibited antibiofilm activity without showing toxicity to the mammalian and microbial cells, highlighting the potential of the enzyme for in vivo applications.

Klebsiella pneumoniae is a gram-negative opportunistic pathogen and a major cause of nosocomial infections such as pneumonia, urinary tract infections (UTI), bacteremia, liver abscess, meningitis, etc. The recent upsurge in antimicrobial resistance among *K. pneumoniae* isolates, and the emergence of highly invasive hypervirulent strains limit the available treatments for *K. pneumoniae* infections[1,2]. Most *K. pneumoniae* strains produce biofilms, in which microorganisms are protected within the self-produced extracellular polymeric substances (EPS), which mainly comprise polysaccharides, extracellular DNAs (eDNAs), lipids, and proteins[3–5]. The dense EPS matrix limits the activity of immune cells[6] and increases the necessity of the dose of certain antibiotics up to 1000 times[7]. Microbes in the biofilm exhibit various altered phenotypes, such as the presence of persister cells, slow metabolic and growth rates, and high rates of horizontal gene transfer, which result in the emergence of multidrug-resistant strains. Many hypervirulent *K. pneumoniae* are hypermucoviscous and often produce a thick mucoid polysaccharide capsule, thereby enhancing the microorganism's ability to elude the host immune response[8–11]. Such properties make *K. pneumoniae* the next global 'superbug' in waiting, and the World Health Organization (WHO) has enlisted it as a critical threat pathogen[3–5,12], highlighting the need for effective strategies for preventing and treating *K. pneumoniae* biofilm-associated infections.

Success against multidrug-resistant microbes invariably requires effective dispersion of biofilms under physiological conditions. The major component of the EPS matrix of biofilm is polysaccharides that provide immense strength and inertness to biofilm. Furthermore, polysaccharides act as nutrient reservoirs and facilitate the formation of a suitably structured environment for microbes to persist[13]. Therefore, the degradation of polysaccharides could substantially weaken the biofilm, leading to easy access of microbes to antimicrobials. Enzymatic dispersion of biofilms has great promise in developing a novel therapy against biofilms since enzymes are biocompatible, and biofilm-associated pathogens are unlikely to develop resistance against enzymes as enzymes do not target the pathogen[14–18]. However, sustained enzyme activity and stability are prerequisites under physiological conditions and in vivo milieu to utilize enzymes for biofilm dispersion in healthcare settings.

The bovine rumen microbial community produces numerous hydrolase enzymes that facilitate the breakdown of complex polysaccharides into simpler sugars under physiological conditions[19–21]. In this regard, there is an ingenious scope for utilizing bovine rumen enzymes for biofilm dispersion. We hypothesized that the bovine mesophilic glycoside hydrolases (GHs), which have naturally evolved from the biomass-degrading microbial communities, would exhibit high saccharolytic activity under physiological

[1]Department of Inorganic and Physical Chemistry, Indian Institute of Science, Bangalore, Karnataka, India. [2]Department of Microbiology and Cell Biology, Indian Institute of Science, Bangalore, Karnataka, India. [3]Molecular Biophysics Unit, Indian Institute of Science, Bangalore, Karnataka, India. [4]School of Biology, Indian Institute of Science Education and Research, Thiruvananthapuram, Kerala, India. ✉e-mail: dipa@iisc.ac.in; debasisdas@iisc.ac.in

conditions. Therefore, these enzymes would be suitable for dispersing polysaccharides of the biofilm matrix under therapeutically relevant conditions.

Here, we present the discovery of the remarkable ability of a bovine rumen microbial enzyme to rapidly disperse the mature biofilms of four different clinical isolates of *K. pneumoniae* from different patients. We establish that the enzyme exhibits unusually high stability, activity, and exceptional ability in dispersing mature *K. pneumoniae* biofilms at a low micromolar concentration under physiological conditions. We explored the mode of biofilm dispersion of the enzyme and established that the enzyme rapidly degrades the matrix polysaccharides. Furthermore, we demonstrate that the enzyme synergistically enhances the antibiotic and immune cell efficacy against the biofilm-encased pathogen and assists in antibiotic treatment of biofilm-associated *K. pneumoniae* infection in mice. By targeting and eradicating biofilms, the enzyme offers a promising biocompatible strategy to overcome the persistent and resistant nature of *K. pneumoniae* infections, unfolding new possibilities for utilizing bovine rumen microbial enzymes against biofilm-associated infections that are a global crisis.

Results

Selection of the bovine microbial enzyme for biofilm dispersion

We analyzed the phylogenetic relationships of 90 GHs of the bovine rumen microbiome (discovered in a previous study[19]) and found that these enzymes primarily belong to the families GH3, GH5, GH8, GH9, GH10, GH26, and GH48 (Fig. 1a). Since cellulosic polysaccharides are the major components of biofilms of many pathogens, we targeted the enzymes of the GH5 family, which are known to act on cellulosic substrates. To refine our selection, we performed domain analysis of the predicted GH5 family of enzymes and identified a putative GH comprising two BACON (Bacteroidetes-Associated Carbohydrate-binding, Often N-terminal) domains along with the GH5 catalytic domain (Fig. 1a, b). The BACON domains are suggested to have the ability to bind to carbohydrates and glycosylated proteins, which might aid in the enzyme's access to the substrate and efficacy in polysaccharide degradation[22]. We named our selected enzyme GH-B2, where B2 stands for the two BACON domains. We analyzed the AlphaFold-predicted structure of the enzyme[23] and found that the BACON domains are majorly comprised of anti-parallel β-sheets. The enzyme displays the (β/α) 8-barrel structure in line with the folding of the GH5 family of enzymes (Supplementary Fig. 1). We further performed multiple sequence alignment of GH-B2 with the well-characterized GH5 enzymes and found that the active site of the enzyme harbors two conserved catalytic glutamate residues, Glu370 and Glu510 (Fig. 1b and Supplementary Fig. 2).

GH-B2 is a potent polysaccharide-degrading enzyme

We successfully expressed GH-B2 in *E. coli* and purified it to homogeneity for the first time (Fig. 1c). The enzyme eluted as a single peak on the size exclusion chromatography column, suggesting its monodisperse and monomeric nature (Fig. 1d). We performed activity assays of GH-B2 with carboxymethyl cellulose (CMC) that closely mimics the natural cellulosic polysaccharides. GH-B2 exhibited high activity with CMC, with the turnover numbers reaching 2872 min^{-1} (Fig. 1e). The enzyme was also active against galactomannan and the model substrates *p*-nitrophenyl-*β*-D-glucopyranoside and *p*-nitrophenyl-*β*-D-galactopyranoside (Supplementary Fig. 3 and Supplementary Table 1). GH-B2 exhibited activity in a wide range of pH (~4.5–10), with maximal activity in the pH range of 5.5–7 (Fig. 1f). The enzyme displayed high activity with CMC at 37 °C; nevertheless, with CMC, the highest activity was observed at 60 °C (Fig. 1g), which could be due to the enhanced solubility and reduced viscosity of CMC at the higher temperature. Moreover, GH-B2 exhibited nearly maximal activity for ~28 days at 37 °C, suggesting a long life of the enzyme under physiological conditions (Fig. 1h). Alongside, the thermal stability of GH-B2 was analyzed, and the T_{50} (the temperature at which the enzyme retains 50% of initial activity) of GH-B2 was found to be ~50 °C (Fig. 1i), suggesting enhanced thermal stability of the enzyme despite being of mesophilic origin. Additionally, GH-B2 maintained ~50% activity in 20% ionic liquid, 1-ethyl-3-methylimidazolium acetate (Fig. 1j), demonstrating remarkable stability of the enzyme. GH-B2 also showed high halotolerance and maintained nearly maximal activity up to at least 2 M NaCl and KCl (Supplementary Fig. 4a). We further tested whether the enzyme undergoes product inhibition and found no effect of glucose and galactose at high concentrations on GH-B2 activity (Supplementary Fig. 4b).

GH-B2 rapidly degrades mature *K. pneumoniae* biofilms

Based on the high activity and stability of GH-B2, we hypothesized that the enzyme could effectively degrade the exopolysaccharides of the biofilm matrix under physiological conditions. Therefore, we investigated the biofilm dispersion ability of GH-B2 against biofilms of several pathogens. In particular, we focused on the biofilms of the members of the ESKAPE pathogens, such as *Klebsiella pneumoniae* (KP 529), methicillin-resistant *Staphylococcus aureus* (MRSA), *Enterobacter aerogenes* (EA), and *Pseudomonas aeruginosa* (PA) and found that GH-B2 effectively disperses the biofilm of *K. pneumoniae* compared to the biofilms of other pathogens (Supplementary Fig. 5). We subsequently tested the efficacy of GH-B2 against biofilms of three more clinical *K. pneumoniae* isolates (KP 20275, KP 5957, KP 6070) from different sources and patients of varying ages and genders (Supplementary Table 2). The whole genome sequencing and multilocus sequence typing (MLST) analyses indicated that the four *K. pneumoniae* isolates were distinct in terms of serotype, clonal type, having different capsular polysaccharides, and virulence genes (Supplementary Table 3). Interestingly, GH-B2 readily dispersed the mature biofilms of all the *K. pneumoniae* isolates (Fig. 2a, b). Among the four, KP 529 and KP 6070 isolates were more virulent and possessed hypermucoviscous genotypes (Supplementary Table 3). However, the phenotypic characterization studies highlighted that KP 6070 was a poor biofilm-producing isolate and the KP 529 was hypermucoviscous and formed a robust biofilm (Fig. 2c and Supplementary Fig. 6). Therefore, the KP 529 isolate was subjected to further studies. The dose titration study showed that GH-B2 could disrupt 3-day-old mature KP biofilm within 2 h with the half-maximal effective concentration (EC_{50}) of 1.94 μM (Fig. 2d). To validate that the dispersion of KP biofilm is due to the degradation of the polysaccharides of the EPS matrix, we isolated the exopolysaccharides of KP biofilm and treated it with GH-B2 and the released sugar was analyzed by gas chromatography coupled to mass spectrometry (GC–MS). We found that glucose was released as the major sugar (retention time: 14.9 min, Fig. 2e and Supplementary Fig. 7). Further, we quantified the amount of glucose released as a function of time using the phenol–sulfuric acid method. We observed a time-dependent gradual release of the sugar from the matrix upon treatment with GH-B2 (Fig. 2e), demonstrating the saccharolytic activity of GH-B2 on exopolysaccharides of *K. pneumoniae*, resulting in KP biofilm disruption.

Interestingly, we observed that GH-B2 could also prevent the formation of KP biofilm over 3 days with a half-maximal concentration (IC_{50}) of 2.50 μM (Fig. 2f). The biomass of *K. pneumoniae* biofilm grown in the presence of GH-B2 was significantly lower than the biofilm grown in the absence of the enzyme (Fig. 2g and Supplementary Fig. 8). Moreover, we observed the segregated cells majorly with very few intercellular connections in the GH-B2 incubated samples (Fig. 2h). We examined whether the biofilm prevention activity of GH-B2 is due to its toxicity on the planktonic *K. pneumoniae* cells or its ability to modify the bacterial surface. However, we did not observe a significant change in the growth of the cells in the presence of GH-B2, which was monitored by analyzing the growth curve of KP and quantifying the number of viable cells at the endpoint (Fig. 2i and Supplementary Fig. 9). Further, the intact surface morphology of the planktonic cells, insignificant changes in their zeta potential, and similar biofilm growth in the presence of GH-B2 suggested that the enzyme does not affect the KP cells (Fig. 2i and Supplementary Fig. 9). These results demonstrate the striking ability of the enzyme to degrade exopolysaccharides, which plays a crucial role in biofilm development and maturation. We subsequently analyzed biofilm dispersion by confocal laser scanning microscopy (CLSM) after staining the samples with texas red conjugated

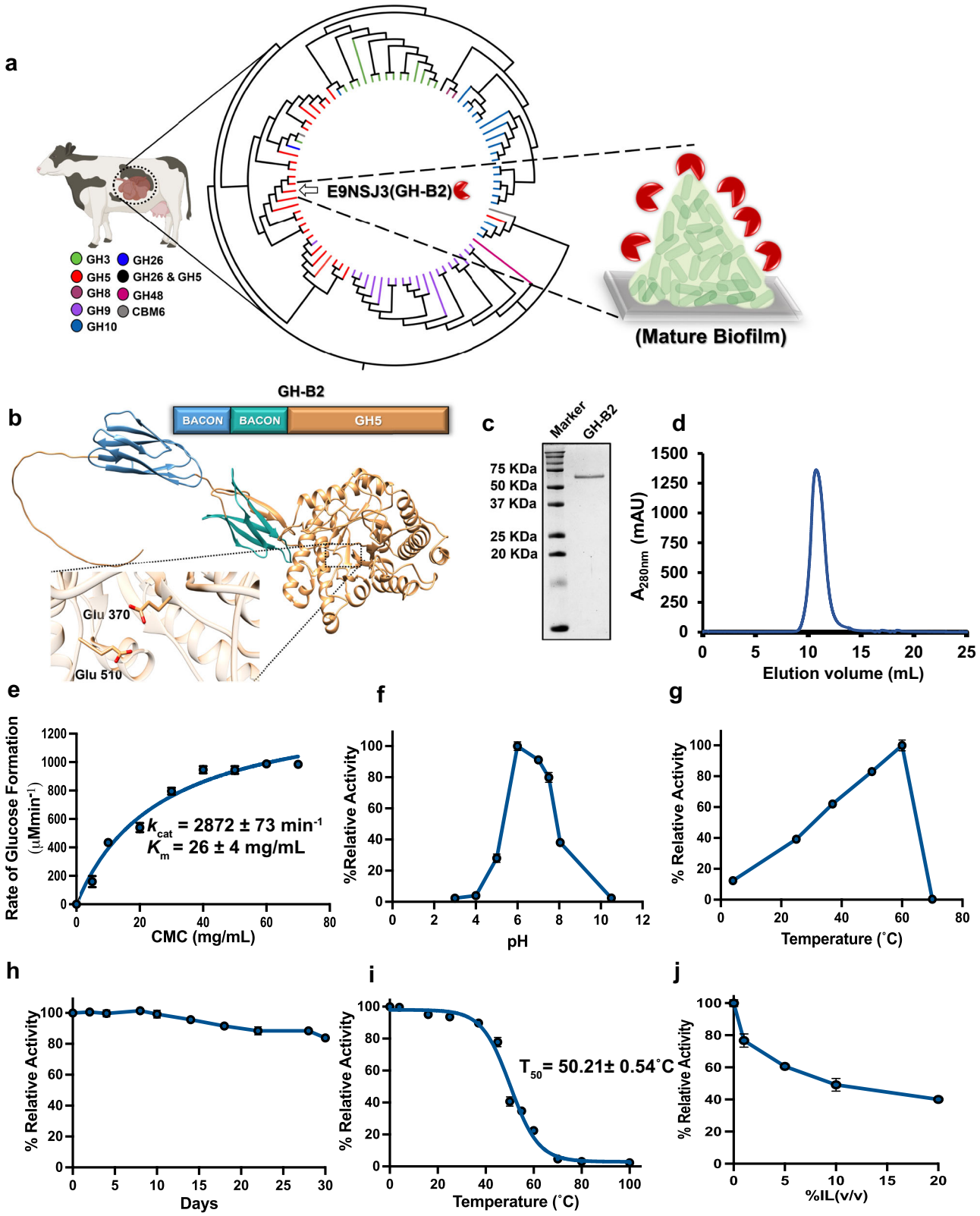

Fig. 1 | Characterization of GH-B2. a Phylogenetic tree of the 90 predicted GHs found in the cow rumen microbiome using maximum parsimony, created using Clustal Omega[59] and analyzed with iTOL (Interactive Tree Of Life software, version 6.9.1) tool[60]. Each clade color indicates a particular GH family. Our selected enzyme GH-B2 (UniProt ID: E9NSJ3) is marked with an arrow. **b** The AlphaFold2-predicted structure of GH-B2[23]. The zoomed-in view of the active site of GH-B2 displays the conserved catalytic residues, Glu370 and Glu510. **c** SDS–PAGE analysis of the purified GH-B2. **d** Size exclusion chromatography (SEC) elution profile of GH-B2. **e** Michaelis–Menten kinetics of GH-B2 with CMC. **f** Relative activity of GH-B2 at different pHs. **g** Relative activity of GH-B2 at different temperatures. **h** Relative activity of GH-B2 as a function of time monitored till 30 days at 37 °C. **i** Thermal stability measurement of GH-B2. **j** Relative activity of GH-B2 at different concentrations of the ionic liquid 1-ethyl-3-methylimidazolium acetate. The observed maximum activity is defined as 100%. All experiments were performed in triplicate ($n = 3$). Error bars correspond to mean ± standard deviation (SD).

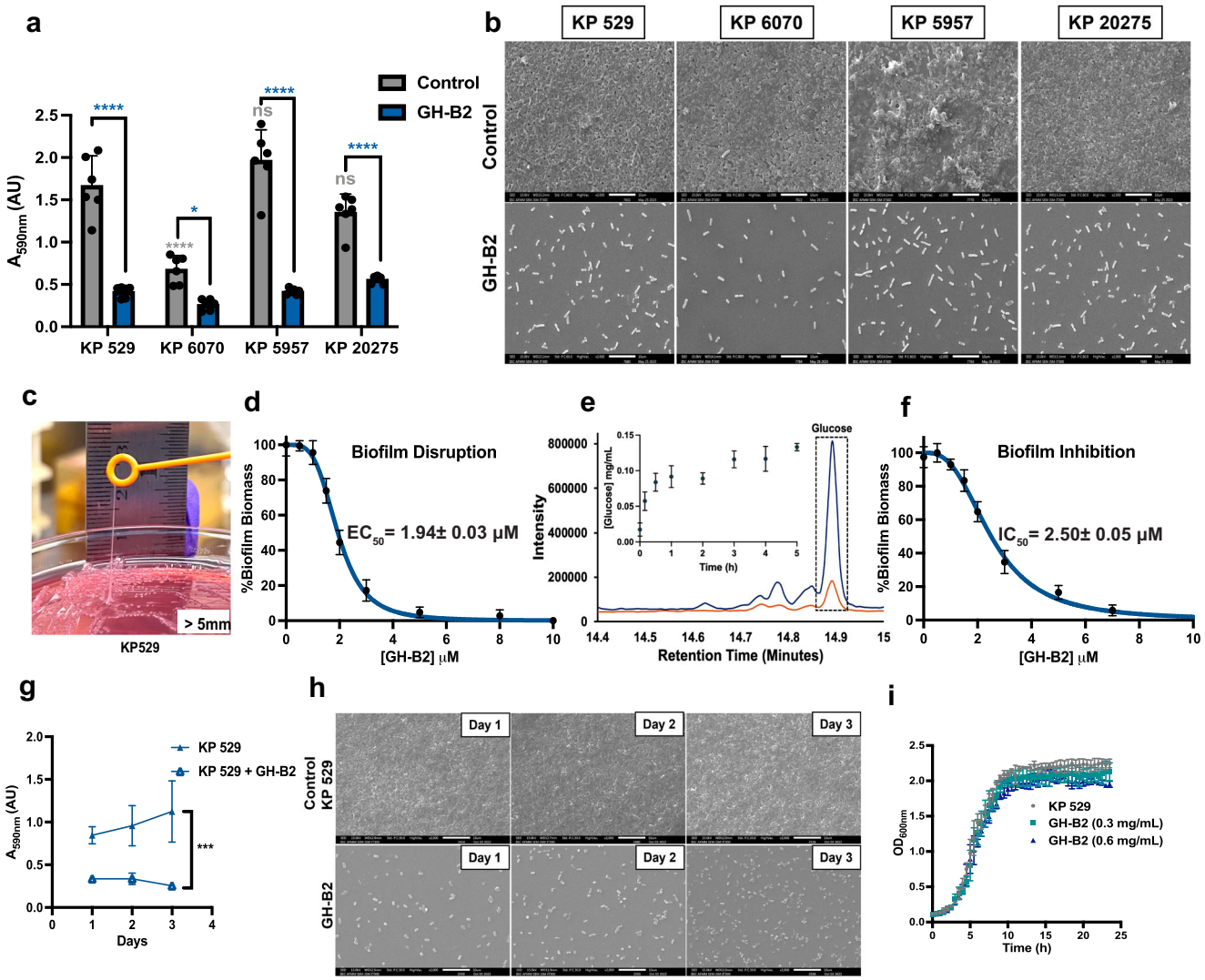

Fig. 2 | GH-B2 prevents biofilm formation and degrades mature *K. pneumoniae* biofilms. a Quantification of biomass of 3-day-old mature biofilm formed by various clinical isolates of *K. pneumoniae* in the absence of GH-B2 (control) and after incubation with GH-B2 (0.3 mg/mL) for 2 h at 37 °C. **b** Scanning electron microscopic (SEM) images of 3-day-old mature biofilms formed by various clinical isolates of *K. pneumoniae* (control) and the corresponding images after incubation with GH-B2 (0.3 mg/mL) for 2 h at 37 °C, scale bar: 10 µm. **c** Overnight incubated *K. pneumoniae* (KP 529) on MacConkey agar plate exhibiting hypermucoviscous thick biofilm. **d** GH-B2 dose-dependent disruption of the 3-day-old mature KP 529 biofilm in 2 h at 37 °C. **e** Sugar release from EPS of *K. pneumoniae* biofilm by GH-B2 at 37 °C. Overlaid gas chromatographs of derivatized samples of EPS with (blue) and without (orange) GH-B2. Silylated glucose *O*-methyl oxime peak (retention time: 14.9 min) is highlighted in a box. The inset shows the amount of glucose released with time. **f** GH-B2 dose-dependent inhibition of KP 529 biofilm formation. Biofilm biomass was quantified after 3 days post-incubation. EC_{50} and IC_{50} values were calculated using nonlinear least-squares fitting to a dose-response model in GraphPad Prism (version 10.1.1) software. **g** KP biofilm formation on a glass coverslip in the absence (control, KP 529) and presence of GH-B2 over 3 days. The biomass quantification was done using the crystal violet (CV) staining assay, and the error bars indicate the standard deviation of $n = 6$ data. Statistical significance was evaluated relative to control using one-way ANOVA with Dunnet's post-hoc test to analyze the data; p values ****<0.0001, ***<0.001, *<0.05. **h** SEM images of KP biofilm formation on a glass coverslip in the absence (control) and presence of GH-B2 over 3 days, scale bar: 10 µm. **i** The growth curve of *K. pneumoniae* in the presence of GH-B2 (0.3 mg/mL and 0.6 mg/mL). The absorbance of the culture (OD_{600}) was measured every 30 min over 24 h. Error bars indicate the standard deviation of triplicate ($n = 3$) data. Representative SEM images were shown.

with Concanavalin A. We observed a gradual depletion in the fluorescence intensity of the dye with the increasing enzyme concentration in the biofilm (Fig. 3a). At 0.3 mg/mL (5 µM) GH-B2, ~85% depletion of fluorescence was observed, suggesting substantial degradation of the polysaccharides of the biofilm (Fig. 3b). We subsequently analyzed the number of viable cells remaining in the biofilm and dispersed to the supernatant after the enzyme treatment. We observed a 4.4 $\log_{10}$ reduction in the surface-adhered bacteria and a 4.15 $\log_{10}$ increase in the viable cells in the supernatant as a result of the enzyme treatment of the biofilm (Fig. 3c). We further evaluated the biofilm dispersion efficacy of GH-B2 as a function of time and found that the enzyme was able to degrade ~90% polysaccharides of KP biofilm in 2 h (Fig. 3d, e). Moreover, the colony formation unit (CFU) analysis showed a 3.41 $\log_{10}$ reduction and a 4.42 $\log_{10}$ increase in the number of viable cells on the surface and the supernatant, respectively (Fig. 3f). These results demonstrate the high efficacy of GH-B2 in degrading the polysaccharides of the EPS matrix of 3-day-old mature *K. pneumoniae* biofilm.

Next, we investigated the effect of GH-B2 on dual-species and polymicrobial biofilms. For this purpose, we employed methicillin-resistant *S. aureus* (MRSA) and *P. aeruginosa* (PA) along with *K. pneumoniae*. We also compared the biofilm dispersion ability of GH-B2 with commercially available glycoside hydrolases- α-amylase and cellulase used at 5 mg/mL, which is ~16-fold greater than the concentration of GH-B2 used. We found that GH-B2 treatment led to ~68% degradation of the polysaccharides in the dual-species biofilm and ~86% degradation in the polymicrobial biofilm.

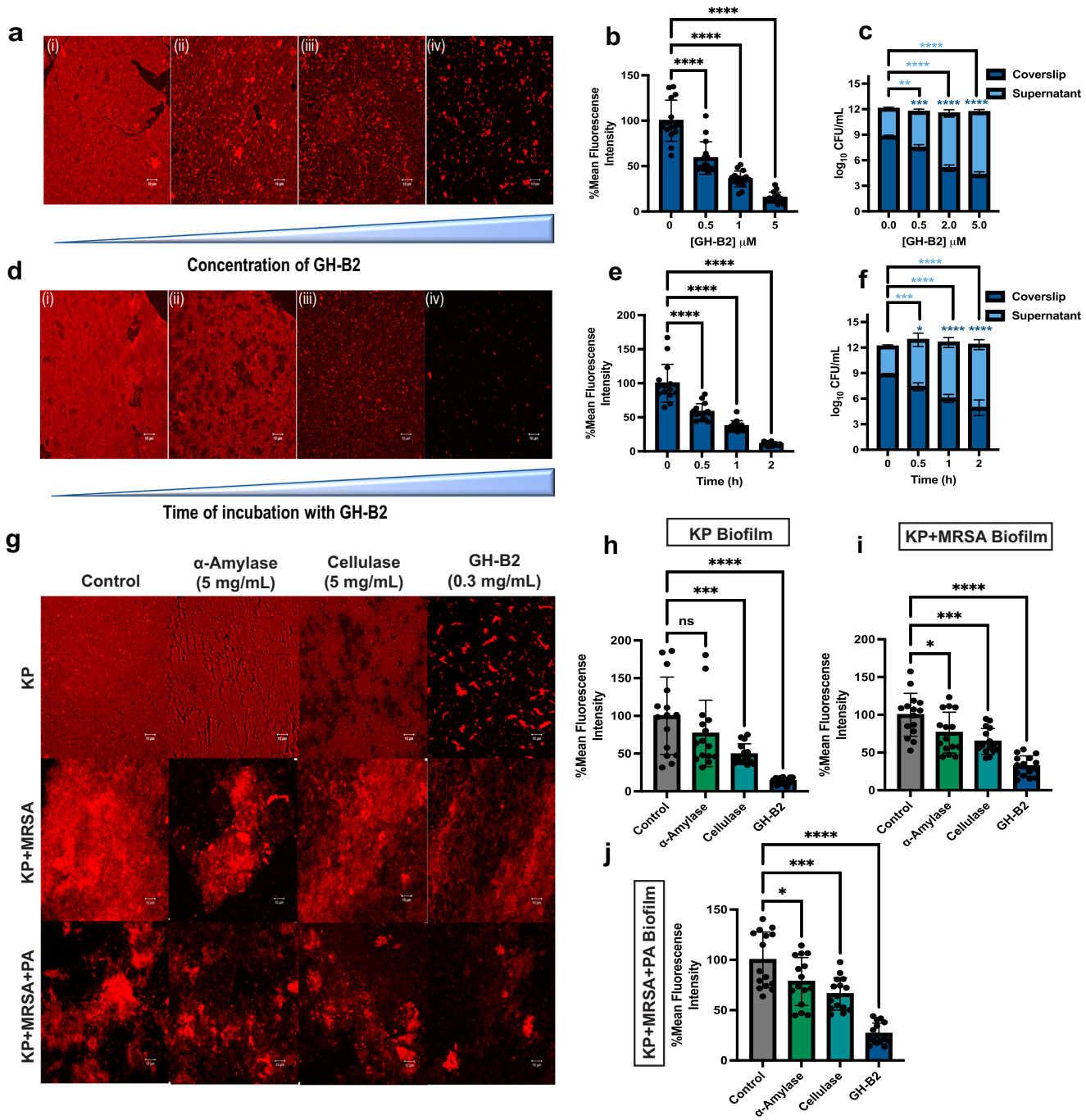

Fig. 3 | CLSM analysis of GH-B2 mediated degradation of polysaccharides of the mature *K. pneumoniae* biofilms. a Dispersion of *K. pneumoniae* biofilm as a function of the concentration of GH-B2. (i) Untreated (ii) 0.03 mg/mL (iii) 0.06 mg/mL, and (iv) 0.3 mg/mL GH-B2-treated 3-day-old biofilm. The enzyme treatment was carried out for 2 h at 37 °C. Corresponding **b** confocal image analysis and **c** CFU in the supernatant and the remaining biofilm on the glass coverslip, $n = 3$. **d** dispersion of *K. pneumoniae* biofilm as a function of time. (i) Untreated (ii) 30 min (iii) 1 h, and (iv) 2 h GH-B2 (0.3 mg/mL)-treated 3-day-old biofilm at 37 °C. Corresponding **e** confocal image analysis **f** CFU in the supernatant and the remaining biofilm on the glass coverslip **g** comparison of the biofilm dispersal activity of α-amylase (5 mg/mL), cellulase (5 mg/mL), and GH-B2 (0.3 mg/mL) on *K. pneumoniae* (KP), KP+ methicillin-resistant *S. aureus* (MRSA), KP + MRSA + *P. aeruginosa* (PA) biofilms, respectively. Corresponding confocal images analysis **h** KP **i** KP + MRSA **j** KP + MRSA + PA. Biofilm was stained with the Texas red conjugated with Concanavalin A, and representative confocal images of maximum intensity projection of Z-stacks are shown, scale bar: 10 μm. For confocal image analysis, each bar indicates mean ± standard deviation. Five confocal images were analyzed from each of three biological replicates, $N = 3$. Statistical significance was evaluated relative to control using one-way ANOVA with Dunnet's post-hoc test to analyze the data; p values ****<0.0001, ***<0.001, **<0.01, *<0.05, ns no significant difference.

However, cellulase, which also targets the β-1,4 glycosidic linkage, could only achieve a ~50% reduction in KP biofilm and KP + MRSA + PA polymicrobial biofilm and ~35% reduction in KP + MRSA dual-species biofilm. Of note, α-amylase displayed very poor ability to degrade polysaccharides of KP biofilm, ~25% reduction observed in KP biofilm, dual-species biofilm, and polymicrobial biofilm (Fig. 3g–j).

To gain insights into the morphological changes of biofilm upon enzyme treatment, we performed scanning electron microscopy (SEM)

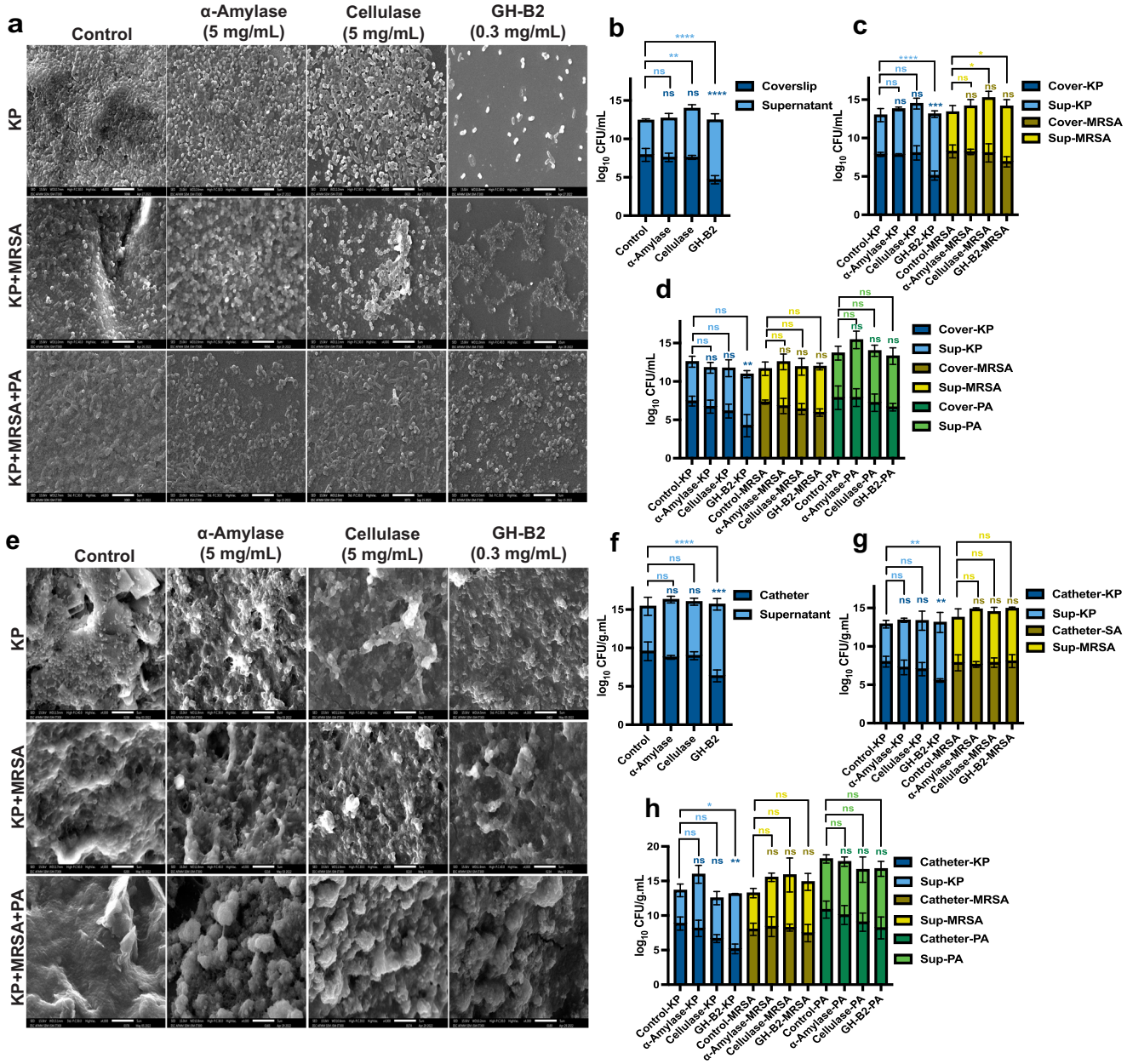

Fig. 4 | SEM analysis of GH-B2-mediated degradation of polysaccharides of the mature *K. pneumoniae* biofilms. SEM images of the biofilm dispersal activity of cellulase (5 mg/mL), α-amylase (5 mg/mL), and GH-B2 (0.3 mg/mL) on *K. pneumoniae* (KP), KP + methicillin-resistant *S. aureus* (MRSA), KP + MRSA + *P. aeruginosa* (PA) biofilms, respectively, grown **a** on glass coverslips, **b–d** corresponding number of CFU in the supernatant and number of CFU remaining in the biofilm; **e** on Foley catheter, **f–h** corresponding number of CFU in the supernatant and number of CFU remaining in the biofilm. All experiments were performed in triplicate ($n = 3$), and representative images were shown, scale bar: 5 µm. Statistical significance was evaluated using two-way ANOVA with Tukey's post-hoc test to analyze the grouped data; p values ****<0.0001, ***<0.001, **<0.01, *<0.05, ns no significant difference.

studies. We observed that in all cases (mono, dual, and polymicrobial biofilms), cells were interconnected through an intertwined thick biofilm matrix (Fig. 4a). When the KP biofilm was treated with GH-B2, the matrices were dispersed, and more segregated cells were observed (Fig. 4a). The corresponding number of viable cells in CFU analysis showed 3.5 $\log_{10}$ reduction in bacterial load compared to control (Fig. 4b). The extent of biofilm dispersion by GH-B2 was found to be moderate for KP + MRSA biofilm and polymicrobial biofilm (KP + MRSA + PA), where GH-B2 could achieve 2.5 $\log_{10}$ reduction in number of *K. pneumoniae*. However, no significant difference was observed in the numbers of MRSA and PA in the dual-species and polymicrobial biofilms after GH-B2 treatment. Of note, the effects of cellulase and α-amylase were non-significant on KP, KP + MRSA, and KP + MRSA + PA biofilms (Fig. 4c, d).

Further, to explore the effect of GH-B2 on medical-device-associated biofilms, we grew 3-day-old mature biofilms on the Foley catheter, treated it with GH-B2, and analyzed the biofilm dispersion via SEM and CFU analysis. We observed a significantly greater amount of biofilm formation on the Foley catheter compared to the glass coverslip surface (Fig. 4e, f). Furthermore, we attempted to measure the thickness of the biofilm formed on the glass coverslip and Foley catheter by scanning electron microscopy using vertical stubs. However, an uneven layer of biofilm formed on the surface, and the difficulty in differentiating between the biofilm and the latex material of the Foley catheter made the measurement challenging (Supplementary Fig. 10). Nevertheless, upon treatment of the biofilms with GH-B2, α-amylase, and cellulase, we observed similar trends of biofilm dispersal on the catheter as on the coverslip. The bacterial load was significantly

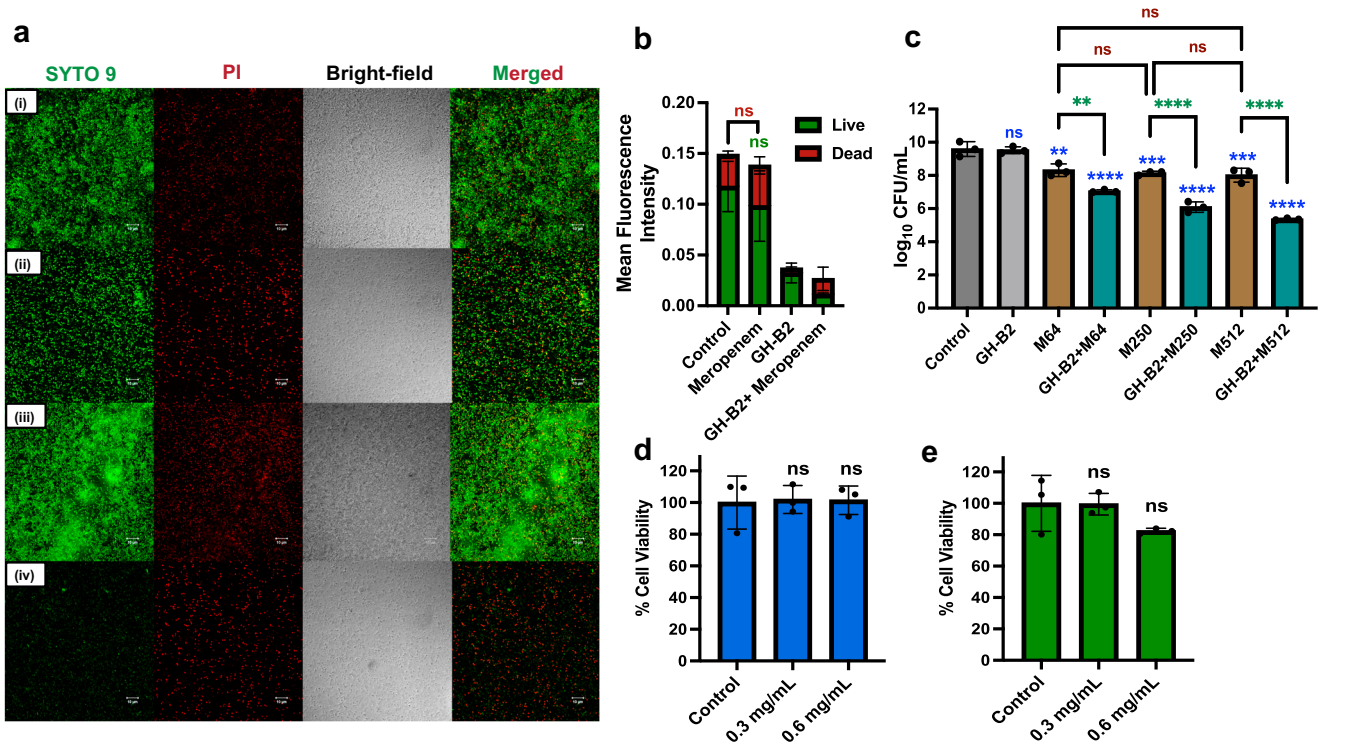

Fig. 5 | GH-B2 enhances the antibiotic efficacy against biofilm-associated *K. pneumoniae*. **a** The biofilm was grown for 3 days and subjected to the combined treatment with GH-B2 and meropenem. CLSM images of (i) phosphate-buffered saline (PBS)-treated, (ii) GH-B2 (0.3 mg/mL)-treated, (iii) meropenem (250 μg/mL)-treated, and (iv) GH-B2 (0.3 mg/mL) + meropenem (250 μg/mL)-treated KP biofilm. The biofilm was subjected to 2 h GH-B2 treatment followed by 24 h meropenem treatment at 37 °C. Green (Syto 9-labeled) cells denote the live cells and red (propidium iodide-labeled) cells with damaged membranes. **b** Corresponding confocal images analysis. **c** CFU analysis of post 2 h GH-B2 treatment followed by 24 h meropenem treatment at 37 °C. M meropenem, and the number following M represents the antibiotic concentration in μg/mL. Statistical significance was evaluated relative to control (blue), meropenem (red), and GH-B2 + meropenem (green) using two-way ANOVA with Tukey's post-hoc to analyze the grouped data; *p* values ****<0.0001, ***<0.001, **<0.01, ns no significant difference. Cytotoxicity analysis of GH-B2 on **d** HeLa cells and **e** macrophage (RAW264.6) upon treatment with GH-B2 (0.3 and 0.6 mg/mL) for 12 h at 37 °C. All experiments were performed in triplicate ($n = 3$), and representative confocal images were shown, scale bar: 10 μm. For confocal image analysis, each bar indicates mean ± standard deviation. Five confocal images were analyzed from each of the two biological replicates, $N = 2$. Statistical significance was evaluated relative to PBS control using one-way ANOVA with Dunnett's post-hoc test to analyze the data; *p* values ****<0.0001, ***<0.001, **<0.01, *<0.05, ns no significant difference.

reduced (3.21 $\log_{10}$ reduction) in GH-B2 treated KP biofilm (Fig. 4f). Similarly, GH-B2 treated KP + MRSA and KP + MRSA + PA catheter biofilms showed 2.8 $\log_{10}$ and 4.1 $\log_{10}$ reduction in number of viable *K. pneumoniae*, respectively. However, the numbers of MRSA and PA cells were non-significant compared to the control samples (Fig. 4g, h). The cellulase and α-amylase remained inactive in KP, KP + MRSA, and KP + MRSA + PA biofilms on the catheter.

GH-B2 enhances antibiotic efficacy against biofilm-associated *K. pneumoniae*

To explore whether GH-B2 can potentiate antibiotics against the biofilm-associated pathogen, we chose meropenem, a broad-spectrum antibiotic. Before employing meropenem, we tested whether the antibiotic had any effect on GH-B2 and found that the antibiotic did not affect the enzyme activity (Supplementary Fig. 11). We then studied the resistance of the planktonic KP to meropenem by measuring the antibiotic's MIC (minimum inhibitory concentration) and found it to be ~4 μg/mL (Supplementary Fig. 12). Interestingly, the MBEC (minimum biofilm eradication concentration) of meropenem was found to be ~500 μg/mL, suggesting poor penetration of meropenem in KP biofilm or its inactivation in the matrix. Meropenem treatment in the presence of GH-B2 (0.3 mg/mL) decreased the viability of the biofilm-encased KP significantly, and the MBEC of meropenem was reduced to ~32 μg/mL. Further, to our surprise, when the KP biofilm was grown in the presence of GH-B2, the MBEC of meropenem was ~2 μg/mL, suggesting that the enzyme prevented biofilm formation, rendering KP cells accessible to the antibiotic (Supplementary Fig. 12).

We subsequently performed live/dead cell staining and CLSM imaging to validate antibiotic potentiation. We performed the experiment on a 3-day-old *K. pneumoniae* biofilm. We note that during this time, a subpopulation of bacteria within the biofilm may not be viable due to natural cell death. The PBS-treated mature KP biofilm exhibited a preponderance of green fluorescence corresponding to the aggregated live KP cells, corresponding to ~78% of live cells (green, stained with Syto 9) and ~21% of cells with damaged membranes or the eDNA in the biofilm (red, stained with propidium iodide (PI)) (Fig. 5a.i, b). GH-B2 treatment dispersed the biofilm, and in the remnants of the biofilm that adhered to the sample ~87% of cells were live, and ~12% of cells were with damaged membranes (Fig. 5a.ii, b). Treatment of the biofilm with meropenem (250 μg/mL) did not significantly affect the number of live cells in the biofilm compared to PBS control. Nevertheless, ~70% of live cells and ~29% of cells with damaged membranes were observed, suggesting poor efficacy of meropenem on the biofilm-encased cells (Fig. 5a.iii, b). Interestingly, when the biofilm was treated with meropenem following GH-B2, very few cells were present in the sample, with ~45% of live cells and ~54% of cells with damaged membranes (Fig. 5a.iv, b). Subsequently, we performed CFU analysis to validate the enzymatic potentiation of meropenem against biofilm-encased KP. Both the control (PBS-treated) and GH-B2-treated biofilms showed a substantial number of viable bacteria (9.58 and 9.52 $\log_{10}$ CFU/mL, respectively) (Fig. 5c), suggesting that GH-B2 disintegrates the biofilm and disperses cells without exerting toxicity to KP. Biofilm treated with varying concentrations of meropenem also showed comparable viable cells, suggesting that meropenem had limited access to the biofilm-encased KP even at 512 μg/mL, a

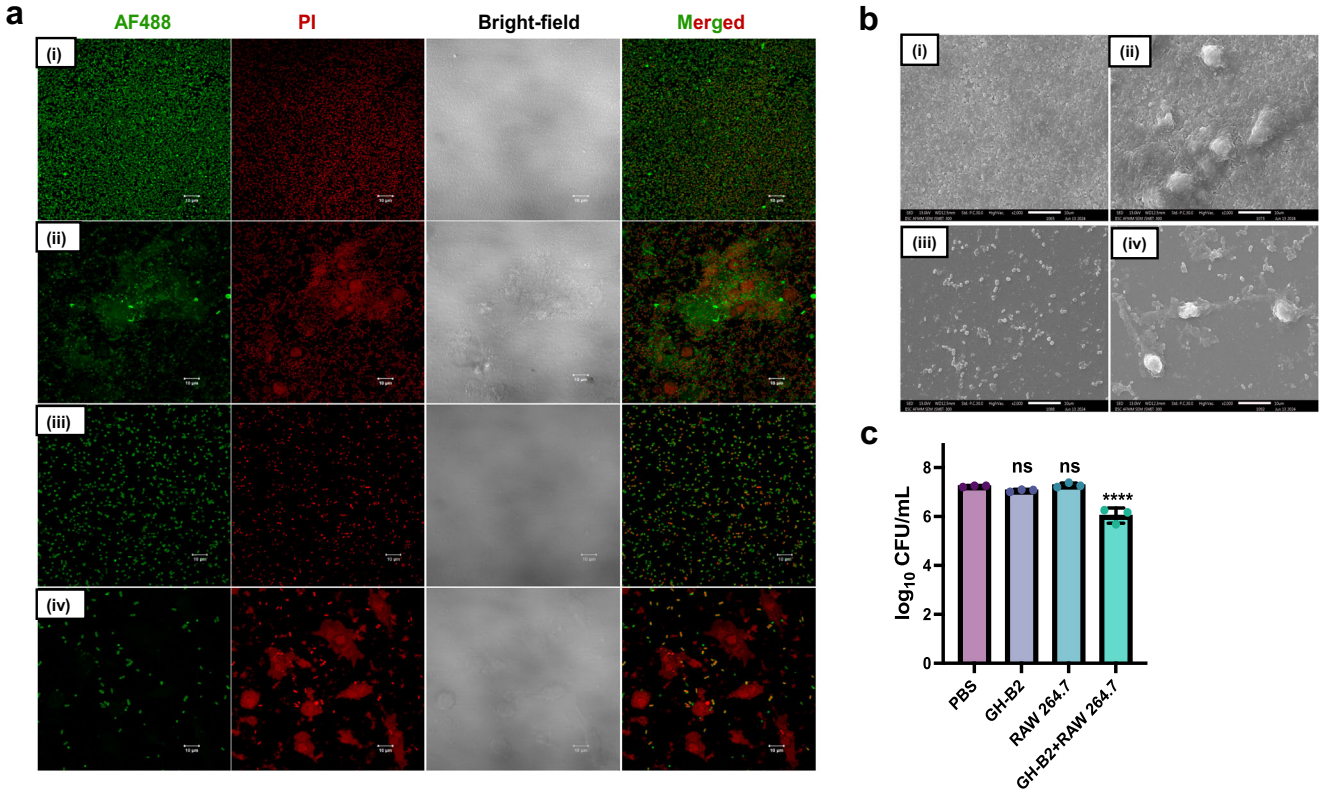

Fig. 6 | GH-B2 enhances the sensitivity of biofilm-encased KP cells to macrophages. The biofilm was grown for 3 days and subjected to the treatment with GH-B2 along with macrophage. CLSM images showing **a** (i) PBS-treated, (ii) macrophage (RAW264.7 cells)-treated, (iii) GH-B2-treated, and (iv) GH-B2 + macrophage-treated KP biofilm, scale bar: 10 µm, AF488 Alexa flour-488, PI propidium iodide. **b** Corresponding SEM images, scale bar: 10 µm. Both the enzyme and macrophage treatments were carried out for 2 h at 37 °C. **c** CFU analysis of post 2 h GH-B2 treatment followed by 2 h macrophage treatment at 37 °C. Experiments were performed in triplicate ($n = 3$), and representative images were shown. Statistical significance was evaluated relative to PBS control using one-way ANOVA with Dunnet's post-hoc test to analyze the data; p values ****<0.0001, ns no significant difference.

concentration 128-fold higher than the antibiotic's MIC of planktonic cells. The population of viable cells was significantly reduced (4.2 $\log_{10}$ reduction) when the biofilm was treated with a combination of GH-B2 and meropenem (512 µg/mL) (Fig. 5c). Additionally, we analyzed the gain of antibiotic resistance of KP in the presence of meropenem alone and combination with GH-B2. We observed enhanced antibiotic resistance in the group treated with meropenem alone from the second generation (G2) onwards. In contrast, the group treated with the combination of GH-B2 and meropenem did not exhibit such enhancement till the third generation (G3) (Supplementary Fig. 13). Taken together, our investigation demonstrates that GH-B2 readily potentiates meropenem against KP encased in the mature biofilm.

Biocompatibility of GH-B2

To explore the feasibility of employing GH-B2 clinically, we examined the biocompatibility of the enzyme toward the human cell line—HeLa and the murine macrophage—RAW264.7 cells. The MTT (3-(4, 5-dimethylthiazolyl-2)-2, 5-diphenyltetrazolium bromide) assay suggested no significant effect of GH-B2 on the HeLa cells (Fig. 5d) and the RAW264.7 cells (Fig. 5e). Further, we explored the stability of GH-B2 in the cell culture media Dulbecco's modified Eagle medium (DMEM) + fetal bovine serum (FBS) and brain heart infusion (BHI) broth and found that the enzyme remains active for 24 h at 37 °C (Supplementary Fig. 14). A major challenge for the enzyme in vivo could be its degradation by the ubiquitous proteases (trypsin-like serine proteases) released by human cells. Therefore, we tested the stability of GH-B2 against trypsin and found that the enzyme retained more than 80% activity up to 3 h and ~50% activity up to 24 h. We also investigated the stability of GH-B2 in mouse serum and human serum and found that the enzyme retained nearly maximal activity in both serums up to 24 h at 37 °C (Supplementary Fig. 14).

GH-B2 enhances immune cell efficacy against biofilm-associated *K. pneumoniae*

Next, we investigated whether the enzyme could potentiate the immune system, such as macrophages and monocytes against the biofilm-encased pathogen. We employed the murine macrophage RAW264.7 cells and human monocyte THP-1 cells against the mature KP biofilm. CLSM and SEM imaging were used to analyze the effect of immune cells (RAW264.7 and THP-1 cells) toward KP biofilm dispersed with GH-B2 (Fig. 6a, b and Supplementary Fig. 15a, b). Both the microscopic data suggested the immune evasion of biofilm-encased KP cells when treated alone with the RAW264.7 cells and THP-1 cells (Fig. 6a.ii, b.ii and Supplementary Fig 15a.iii, b.iii). However, immune cells were able to access the biofilm-encased KP cells after GH-B2 treatment (Fig. 6a.iv, b.iv and Supplementary Fig. 15a.iv, b.iv).

We observed that the macrophage and monocyte could access more KP cells upon treatment of the KP biofilm with GH-B2, which was further confirmed by the reduction in the number of viable cells (Fig. 6c and Supplementary Fig. 15c). Although the effect of 2 and 20 h incubation of RAW264.7 cells alone on KP biofilm was insignificant, on the GH-B2 dispersed samples, 1.20 $\log_{10}$ (2 h incubation with RAW264.7 cells) and 1.69 $\log_{10}$ (20 h incubation with RAW264.7 cells) reduction in the number of KP cells were observed (Fig. 6c and Supplementary Fig. 15f). We also observed similar results for the THP-1 cell treatments. The THP-1 cells alone could not access the biofilm-encased KP cells. However, the number of viable cells was reduced (1.50 $\log_{10}$ reduction) upon treatment of the biofilm with GH-B2, followed by THP-1 cells (Supplementary Fig. 15c). These results demonstrated that GH-B2 could substantially improve the accessibility of the macrophage and monocyte, the vital components of the host immune system, toward the biofilm-encased KP cells.

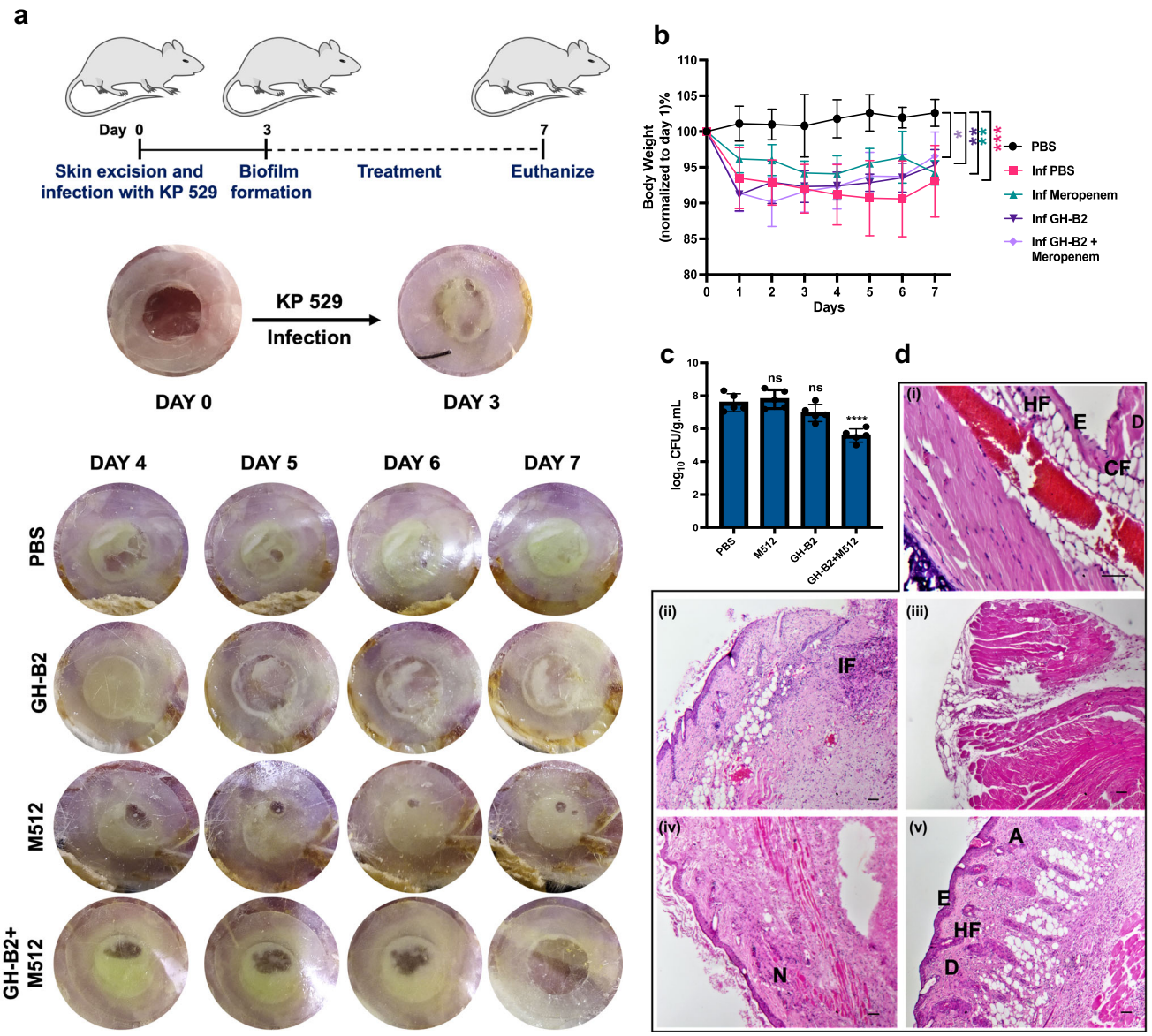

Fig. 7 | GH-B2-mediated treatment of biofilm-associated *K. pneumoniae* infection in mice. a Representative images of different treatment groups—*K. pneumoniae* infected wound with PBS (control), meropenem (512 μg/mL), GH-B2 (0.6 mg/mL), and GH-B2 (0.6 mg/mL) + meropenem (512 μg/mL). **b** Body weight data represent mean ± SD, $n = 5$ mice/group. **c** CFU of *K. pneumoniae* on day 7 after different treatments, $n = 5$. **d** Histopathological analysis of wound tissue using H&E staining at day 7, uninfected (control) wound, PBS-treated, GH-B2 (0.6 mg/mL)-treated, meropenem (512 μg)-treated, and GH-B2 (0.6 mg/mL) + meropenem (512 μg)-treated infected wounds. Scale bar: 50 μm, E epidermis, D dermis, CF collagen fibers, IF inflammatory infiltrates, N necrosis, A angiogenesis, HF hair follicles. Statistical significance was evaluated relative to PBS control using one-way ANOVA with Dunnet's post-hoc to analyze the data; p values ****<0.0001, **<0.01, *<0.05, ns no significant difference.

GH-B2 potentiates antibiotic treatment of biofilm-associated *K. pneumoniae* infection in mice

We subsequently employed a chronic wound infection model in mice to explore the efficacy of the enzyme in vivo. After creating the wound and 3 days of post-infection with KP, we observed the development of a slimy, thick, mature KP biofilm (Fig. 7a). Thereafter, we treated the infection with GH-B2, meropenem, and a combination of the enzyme and the antibiotic, and monitored the infection and the overall health of mice for the next 4 days. In the PBS-treated group and meropenem-treated group, the biofilm increased over time, demonstrating the inability of meropenem to access biofilm-encased KP cells. Upon treatment with GH-B2, the biofilm was significantly depleted, demonstrating the high efficacy of GH-B2 in dispersing the mature biofilm in vivo. However, wound healing was not observed, suggesting that the enzyme did not affect the KP cells, and the infection persisted. Interestingly, the combination of GH-B2 with meropenem significantly reduced biofilm over 4 days of continuous treatment and almost completely cleared on day 7 (Fig. 7a). A daily supervision of the health of mice indicated a 4–7% decrease in the body weight in all infected mice during the initial 3 days compared to the uninfected control group. Afterward, the GH-B2 + meropenem-treated cohort started recovering weight. However, in other groups, the pace of recovery was relatively slow (Fig. 7b), indicating the persistence of infection and pain.

We observed higher KP levels in the wound tissue treated with PBS (7.57 $\log_{10}$ CFU/g.mL) compared to the GH-B2 + meropenem-treated group (5.5 $\log_{10}$ CFU/mL), indicating ~2.1 $\log_{10}$ bacterial load reduction in the GH-B2 + meropenem-treated group of mice. However, only meropenem and GH-B2-treated groups exhibited similar bacterial loads compared to the PBS control (Fig. 7c). We subsequently performed histopathology analysis on wound tissues to qualitatively assess the effect of treatments on day 7. In the KP biofilm-formed group, we observed a

sloughed-off epidermis with poor re-epithelialization and the persistence of abundant inflammatory infiltrate (Fig. 7d). Similarly, we found poor re-epithelialization with abundant inflammatory infiltrate in the wounds treated with GH-B2 or meropenem (Fig. 7d). However, in the wound treated with GH-B2 + meropenem (Fig. 7d), we observed the process of wound healing with a reconstitution of the regular epidermal lining and evident keratinization with variable degrees of re-epithelialization, angiogenesis, and appearance of hair follicles. Together, these results validate the ability of the enzyme to potentiate meropenem against biofilm-associated KP wound infection in vivo.

Discussion

In the current era of antimicrobial drug-resistance, biofilm-associated infections have emerged as a severe threat to human health. Enzymatic dispersion of biofilms via degrading exopolysaccharides of the matrix is a promising strategy to combat biofilm-associated infections[18]. Since cow rumen harbors powerful mesophilic microbial enzymes capable of degrading recalcitrant polysaccharides under physiological conditions, we explored the feasibility of utilizing such an enzyme for dispersing mature biofilms. We identified GH-B2 as a potential polysaccharide-degrading enzyme comprising a catalytic GH domain and two BACON domains, which could assist in effectively binding to polysaccharides[22]. The high catalytic activity and prolonged stability of the enzyme under physiological conditions are attributes essential for a biofilm-dispersing enzyme. Based on the substrate screening, GH-B2 displayed specificity toward β-1,4 linked glucose/galactose/mannose-containing substrates. The enzyme showed high turnovers (k_{cat} 2872 min^{-1}) with CMC, a long-chain polysaccharide with the β-1,4 glycosidic linkage and a close mimic of the cellulosic polysaccharides found in the biofilm matrix of many pathogens[24,25]. Moreover, the enzyme exhibited remarkable stability and desired properties such as high halotolerance and no product inhibition, which is known to rapidly diminish the activity of GH enzymes[26,27], making it a suitable candidate to study biofilm dispersion.

We used four clinical isolates of *K. pneumoniae*, which were isolated from different patients, to check the activity of GH-B2 on their biofilms. The enzyme rapidly dispersed the mature biofilms of all *K. pneumoniae* isolates regardless of their genetic heterogeneity, suggesting good applicability of the enzyme against biofilm-associated KP infections. The string test and the sedimentation assay indicated the hypermucoviscous phenotype of KP 529 isolate among the four isolates tested. Often, hypermucoviscous strains of *K. pneumoniae* are more pathogenic than other strains. These strains produce a thick, slimy capsule that impedes the immune system's ability to recognize and eliminate the bacteria, thereby exhibiting heightened virulence[9,28–30]. Therefore, we focused on GH-B2-mediated dispersion of mature biofilm of hypermucoviscous *K. pneumoniae* (KP 529). First, we monitored the effect of GH-B2 on the EPS polysaccharides of biofilm using confocal imaging by employing Texas red conjugated with concanavalin A, a carbohydrate-binding protein that specifically binds to the polysaccharides of the EPS matrix[31,32]. The concentration and time dependence studies showed that 5 μM of GH-B2 was effective in disintegrating the EPS polysaccharides of KP biofilm in 2 h at 37 °C. Additionally, we compared the efficacy of GH-B2 in dispersing biofilms with cellulase and α-amylase. These two commercially available enzymes have been reported for the biofilm dispersion studies of *S. aureus* and *P. aeruginosa*, albeit used at a very high concentration (5 mg/mL)[17,33]. Interestingly, the comparison of the biofilm dispersion activity of GH-B2 with cellulase and α-amylase revealed that these enzymes were nearly inactive against the KP biofilm even at a concentration ~16-fold higher than GH-B2.

In nature, polymicrobial biofilms are more prevalent, comprised of multispecies and different strains of bacteria that co-exist, and the synergistic interactions promote the development of antibiotic resistance and more robust biofilm[34]. Considering the complexity and relevance of polymicrobial biofilms, we analyzed the effect of GH-B2 on KP + MRSA and KP + MRSA + PA. Our results indicated that GH-B2 could effectively lead to the dispersion of the KP cells from the mature polymicrobial biofilms of KP + MRSA + PA. These three bacteria are the most prevalent ones involved with biofilm formation in chronic wounds and medical-device-related infections and are associated with higher patient fatality rates in intensive care units (ICU)[35]. The superior biofilm dispersion ability of GH-B2 could be attributed to the advantage of GH-B2 harboring BACON domains coupled with the high innate activity and stability of the enzyme originating from the cow rumen. However, GH-B2 failed to disrupt the biofilms formed by MRSA and PA, which could be due to the specificity of GH-B2 toward the β-1,4 linked glucose, mannose, and galactose residues, which is less or absent in the MRSA and PA biofilms. Apparently, the EPS matrix of PA biofilm contains alginate polysaccharides composed of 1–4 linked β-D-mannuronic acid and α-L-glucuronic acid[18]. However, based on the model substrate screening (Supplementary Table 1), GH-B2 was not active on *p*-nitrophenol-β-glucuronide and alginate. Despite the vast literature on the characterization of capsular and lipopolysaccharides, little is known about the polysaccharides in the EPS matrix of KP biofilms. As per the reports, glucose, mannose, galactose, and their amines and acetylated derivatives are present in the polysaccharides of the EPS matrix of KP biofilms[36–38]. The model substrate screening against GH-B2, the GC–MS analysis of GH-B2-treated exopolysaccharide (isolated from KP biofilm), and the dispersed polysaccharides of the GH-B2 treated KP biofilm suggest that GH-B2 possibly targets the β-1,4 linked glucose, mannose, and galactose residues in the KP biofilm matrix.

To explore the activity of GH-B2 toward biofilms in a more clinically relevant setting, we investigated the effect of the enzyme on biofilms produced on the Foley catheter, which is one of the most commonly used indwelling catheters[39] and more susceptible to biofilm formation than silicone catheter[40,41]. In fact, *K. pneumoniae* is one of the pathogens that lead to frequent catheter-associated urinary tract infections[42]. Developing an alternative to antimicrobial coating for medical devices is crucial in the current era of antimicrobial resistance. In this line, previous research demonstrated that bacteriophage can be employed for preventing the colonization of *Klebsiella* and thereby, biofilm formation on urinary catheters[43]. However, the phage encoding depolymerase was unable to eradicate pre-formed mature biofilm, indicating the complexity of the EPS matrix, which results in limited penetration and activity[43]. Based on our study, GH-B2 was more efficient in dispersing the catheter biofilms than cellulase and α-amylase, highlighting its potential applicability against catheter-associated KP infections.

Notably, GH-B2 did not affect the *K. pneumoniae* growth; instead, it inhibited the biofilm formation, plausibly by degrading the in situ generated exopolysaccharides that assist in the initial adhesion and aggregation of bacteria to develop the biofilm. We also note that a phage depolymerase enzyme, Dep42, has been reported to have antibacterial and antibiofilm activity by targeting the specific capsular polysaccharide of *K. pneumoniae*[44]. Also, an endolysin, LysECD7, has been shown to have antibacterial and antibiofilm effects on *K. pneumoniae* biofilm by degrading the peptidoglycan layer of the cell wall[45,46]. However, gram-negative bacteria, such as *K. pneumoniae*, which possess an outer membrane surrounding the cell wall, require a high concentration of endolysin for antibacterial activity. Thus far, to the best of our knowledge, GH-B2 would be the most specific enzyme for *K. pneumoniae* biofilm disassembly and inhibition without being toxic to the planktonic cells.

Another major goal of our investigation was to render existing antibiotics facile access to the biofilm-associated pathogens, thereby facilitating the eradication of the pathogens. The dwindling nature of new antibiotic development has spurred renewed interest in using the existing antibiotics in the best possible ways against bacterial infections[47,48]. We have used meropenem, which belongs to the carbapenem class of antibiotics that inhibits cell wall synthesis in bacteria by strongly binding to penicillin-binding proteins. This clinically relevant broad-spectrum antibiotic often fails to reach the biofilm-encased KP cells due to poor diffusion through the heterogenous EPS matrix and the degradation by the beta-lactamases (especially the extended-spectrum β-lactamases producing *K. pneumoniae*) in the *K. pneumoniae* biofilm[49,50]. This limited penetration can contribute to

the development of antibiotic resistance within biofilm. Besides, meropenem is more effective against the metabolically active cells compared to the dormant bacteria in the biofilm[51–53], making it an ideal candidate to evaluate how enzymatic biofilm dispersion improves antibiotic efficacy. Our study demonstrates that GH-B2 effectively disperses biofilms, releasing more KP cells into the planktonic state. In contrast, the meropenem-treated group showed minimal biofilm disruption, with cells remaining encased in the matrix despite shaking. This highlights a key advantage of GH-B2: dispersing the biofilm and exposing a greater number of susceptible planktonic cells to a uniform concentration of the antibiotic, potentially reducing the selective pressure that promotes resistance development. However, long-time evolution studies and further analysis of the evolved strains, focusing on mutations associated with antibiotic resistance need to be analyzed[54,55]. The CLSM images clearly indicated the inaccessibility of meropenem toward the biofilm-encased KP cells. Moreover, GH-B2 dispersed the majority of cells into the supernatant; therefore, meropenem treatment of the GH-B2 incubated samples displayed only the effect of meropenem on the biomass remaining (a few discrete cells) over the sample surface. However, the CFU analysis validated GH-B2-mediated improved efficacy of meropenem on the biofilm-encased KP cells. Another major challenge associated with biofilm is the immune evasion of biofilm-encased bacterial cells, which often results in chronic infections, tissue damage, and dissemination of infection. We used two different dyes to differentiate macrophage/monocytes (immune cells) and KP cells. What we observed is the effect of macrophages/monocytes toward the remaining biofilm (very few cells) adhered to the surface after biofilm dispersion by GH-B2, as most cells were dispersed into the supernatant. Quantifying the numbers of viable cells indicated no significant reduction in CFU in murine macrophages (RAW264.7 cells) and human monocytes (THP-1 cells) alone on KP biofilm. In contrast, we observed a significant reduction in CFU of KP cells when the GH-B2 dispersed biofilm was treated with the RAW264.7 cells and THP-1 cells. The results were in accordance with the recent report by Guilhen et al., where the engulfment rate of macrophage (RAW264.7 cells) was higher with the cells that got dispersed from KP biofilm (mechanical disruption of KP biofilm), compared to planktonic and sessile cells[56].

In the in vivo model study, the GH-B2 alone-treated group did not exhibit a significant increase in biofilm over time. This suggests that with continuous daily topical application for 4 days, GH-B2 effectively disperses newly formed biofilms (developing within 24 h) and potentially prevents further biofilm formation as long as the enzyme remains in the wound area. We did not observe any bacterial dissemination to blood or any other organs, such as mesenteric lymph nodes, spleen, liver, and lungs, in all cohorts of infected mice. This suggests the dispersed cells remained localized to the skin, trapped under the dressing—an ideal environment for biofilm formation rather than a planktonic, metabolically active state. Consequently, not all cells would have been susceptible to meropenem, potentially explaining the lower reduction of viable cells observed in the GH-B2 + meropenem group compared to the PBS control. However, we observed that the adjuvant activity of GH-B2 with meropenem resulted in rapid clearance of KP biofilm from the mouse wound infection. Moreover, we observed a significant weight loss in mice, especially in the infected groups treated with PBS, meropenem, and GH-B2, which did not recover well over time. The wound infection can cause pain and stress, reducing food intake and subsequent weight loss in mice. In contrast, even though weight loss happened in the group of mice treated with GH-B2 + meropenem in the initial days, it slowly recovered with the treatment, suggesting wound healing, which is further supported by the histopathology data. Taken together, the in vivo studies established that the enzyme improved the antibiotic efficacy against the biofilm-associated *K. pneumoniae* infection in mice, leading to facile clearance of biofilm and initiation of wound healing.

Although the wound model used in this study has previously been successfully applied for screening and development of the antimicrobials on *K. pneumoniae* wound infections[57,58], a limitation of this model in the current study is that the enzymatically dispersed bacterial cells remain localized to the skin, trapped under the dressing—a suitable environment for biofilm formation. Consequently, not all cells would be susceptible to meropenem, potentially explaining the lower reduction of viable cells observed in the GH-B2 + meropenem group compared to in vitro results. Moreover, due to the topical application method in this in vivo model, the prevention of biofilm re-establishment cannot be definitively guaranteed. The duration of enzyme contact with the biofilm is, to some extent, unpredictable as the mice regain mobility shortly after anesthesia. Nevertheless, we envision that a formulation of the enzyme with hydrogel, or its encapsulation into a suitable nanocarrier, would pave the way for its targeted delivery in vivo. Overall, our findings unveil the untapped potential of a cow rumen microbial enzyme for dispersing mature KP biofilms under physiological conditions.

Methods

Bioinformatics analysis

Multiple sequence alignment and phylogenetic tree analyses were carried out using the sequences of 90 putative glycoside hydrolases reported in the discovery of cow rumen microbial glycoside hydrolase enzymes[19]. The protein sequences were obtained from the NCBI database. The multiple sequence alignment was performed using default settings, and a phylogenetic tree was built using the Neighbor-Joining method (the default tree-building method in Clustal Omega)[59]. The results were uploaded to the online tool ITOL[60] (Interactive Tree of Life, version 6.9.1) for visualization and further annotations. The structure of the selected candidate enzyme, GH-B2, was predicted by AlphaFold2[23]. The conserved domains of the protein were located employing Pfam 34.0[61], and the final image was created using Chimera version 1.16. Subsequently, we used the SWISS-MODEL (a web-based automated protein modeling server)[62] to identify putative homologs of the GH-B2.

Recombinant expression and purification of GH-B2

The gene encoding GH-B2 (UniProt ID: E9NSJ3) was synthesized in its codon-optimized form by GenScript, USA, for over-expression in *E. coli*. The gene was cloned into the pE-SUMO vector using BsaI and XhoI restriction enzymes. *E. coli* BL21(DE3) cells were transformed with the plasmid harboring the gene encoding GH-B2. The cells were grown overnight on an LB-agar plate containing 50 μg/mL kanamycin. A single colony was picked from the agar plate and grown overnight in a 5 mL LB culture with the same antibiotic. The resulting overnight culture was transferred to 500 mL LB medium supplemented with 50 μg/mL kanamycin, and the cells were grown at 37 °C. At O.D. 0.6 at 600 nm, protein expression was induced with 0.5 mM isopropyl *β*-D-1-thiogalactopyranoside (IPTG), and the cells were further grown for an additional 20 h at 25 °C with 220 rpm shaking. The cells were harvested by centrifugation at 4000 × *g* for 30 min at 4 °C. The expression of the protein was confirmed by SDS–PAGE analysis. For protein purification, all the steps were carried out strictly at 4 °C. The harvested cells were resuspended in the lysis buffer (100 mM HEPES, pH 7.5, and 300 mM KCl) supplemented with 0.5 mg/mL lysozyme egg white, 0.2 mM PMSF, 5 mM DTT, and 5 μg/mL DNase. The resuspended cells were tumbled for 30 min at 4 °C, followed by sonication (45% amplitude, 1 s on–2 s off, 3 × 45 s) using a sonicator (Q500, Qsonica USA). The suspension was kept on ice for 5 min in between the sonication cycles. The cell lysate was centrifuged at 12,400 × *g* for 45 min at 4 °C. The supernatant was incubated with Ni-NTA resin, which was pre-equilibrated with buffer A comprising 50 mM HEPES, pH 7.5, 300 mM KCl, and 5% glycerol. The mixture was tumbled overnight at 4 °C and transferred to an empty column. The flow-through was discarded, and the resin was washed with a 15-column volume (CV) of wash buffer 1 (50 mM HEPES, pH 7.5, 300 mM KCl, 5% glycerol, and 20 mM imidazole), 15-CV of wash buffer 2 (50 mM HEPES, pH 7.5, 300 mM KCl, and 5% glycerol, and 40 mM imidazole) and 5-CV of wash buffer 3 (50 mM HEPES, pH 7.5, 300 mM KCl, 5% glycerol, and 60 mM imidazole). GH-B2 was eluted with 5-CV of elution buffer (50 mM HEPES, pH 7.5, 300 mM KCl, 5% glycerol, and 300 mM imidazole). The elution fractions were combined and dialyzed using buffer B (50 mM HEPES, pH 7, 300 mM KCl, 10% glycerol). Further, the dialyzed protein was purified by size exclusion chromatography (SEC) using ENrich™ SEC 650 10 × 300

column. After flash freezing in liquid nitrogen, the purified protein was stored in a −80 °C freezer.

The SUMO-tag of the protein was cleaved using SUMO protease, which was expressed and purified in-house using a previously reported protocol[63]. Briefly, the SUMO-tagged protein was incubated with 0.2 equivalent of SUMO protease at 4 °C overnight with slow tumbling at 80 rpm. The solution was incubated with Ni-NTA resin for 2 h, and the flow-through containing the untagged protein was collected. The purity of the protein was analyzed by SDS–PAGE. The concentration of the purified protein was measured from the absorbance of the protein at 280 nm, based on the molar extinction coefficient ($\mathcal{E}_{280}$ = 100,770 M^{-1} cm^{-1}) of the protein at 280 nm (calculated using the ProtParam-Expasy).

Biochemical characterization of GH-B2

The enzymatic activity of GH-B2 was measured using two different assays: 3,5-dinitrosalicylic acid (DNS) assay and *p*-nitrophenol (PNP) assay[64,65]. PBS buffer (8 mM Na_2HPO_4, 2 mM KH_2PO_4, pH 7, 137 mM NaCl, 2.7 mM KCl) was used for all assays unless stated otherwise. Both assays were carried out at 37 °C.

DNS assay. The hydrolytic activity of GH-B2 on carboxymethyl cellulose (CMC), amylose, and chitin was measured using the DNS reagent (44 mM 3,4-dinitrosalicylic acid, 21 mM phenol, 4 mM sodium sulfite, and 250 mM sodium hydroxide). The reaction mixture contained 4% (W/V) CMC and 500 nM enzyme in the assay buffer. Additionally, two control assays devoid of the enzyme and the substrate were carried out. Assays were incubated at 37 °C for 10 min, followed by heating at 100 °C for 5 min to quench the reaction. Subsequently, the DNS reagent was added to the reaction mixture, and the mixture was heated again at 100 °C for 10 min. The mixture was cooled to room temperature (25 °C), and absorbance was recorded at 540 nm using the microplate reader (BioTek Synergy H1). The amount of glucose released in the assay was calculated using the standard calibration curve generated using various known glucose concentrations. Multiple parameters were optimized to determine the optimal activity of GH-B2 with CMC, including pH, temperature, time, and the effect of various additives were monitored using the DNS assay. All measurements were performed at least in triplicates (n = 3).

PAHBAH assay. GH-B2 activity on galactomannan was analyzed using *p*-hydroxybenzoic acid hydrazide (PAHBAH) assay[66]. Briefly, galactomannan was incubated with 0.06 mg/mL of GH-B2 at 37 °C for 30 min, followed by heating at 100 °C for 5 min to quench the reaction. Subsequently, PAHBAH reagent (50 mM PAHBAH, 10 mM bismuth nitrate, 10 mM sodium, potassium tartrate in 0.5 M NaOH) was added to the reaction mixture, and the mixture was heated again at 100 °C for 10 min. The mixture was cooled to room temperature (25 °C), and absorbance was recorded at 405 nm using the microplate reader (BioTek Synergy H1). The amount of mannose released in the assay was calculated using the standard calibration curve generated using various known concentrations of mannose.

PNP assay. These assays contained 2 mM PNP substates (*p*-nitrophenyl-*β*-D-glucopyranoside, *p*-nitrophenyl-*β*-D-galactopyranoside, *p*-nitrophenyl-*α*-D-glucopyranoside, of *p*-nitrophenyl-*N*-acetyl-*β*-D-glucosaminide, *p*-nitrophenyl-*α*-D-maltohexoside, *p*-nitrophenyl-*β*-D-xylopyranoside, and *p*-nitrophenyl-*β*-D-glucuronide) and 0.06 mg/mL GH-B2 in the assay buffer. Assays were incubated at 37 °C for 3 h. Additionally, two control assays devoid of the enzyme and the substrate were carried out. The reactions were quenched by adding an equal volume of glycine–NaOH buffer, pH 10.4, followed by the measurement of absorbance at 400 nm using the microplate reader. The amount of *p*-nitrophenol released in the assay was calculated using the standard calibration curve generated using various known concentrations of *p*-nitrophenol. To determine the optimal activity of the enzyme with PNP substrates, various parameters have been optimized, including pH, temperature, salt, and glycerol.

Enzyme kinetics of GH-B2. Kinetics studies of GH-B2 were carried out using carboxymethyl cellulose (CMC), galactomannan, and the model substrates—*p*-nitrophenyl-*β*-D-glucopyranoside and *p*-nitrophenyl-*β*-D-galactopyranoside. For CMC, the 0.03 mg/mL (0.5 µM) enzyme was incubated with various concentrations of CMC (0–70 mg/mL) in PBS buffer, pH 7 at 37 °C. For galactomannan, the 0.06 mg/mL (1 µM) enzyme was incubated with various concentrations of galactomannan (0–70 mg/mL) in PBS buffer, pH 7 at 37 °C. For the PNP substrates, 0.06 mg/mL enzyme was incubated with various concentrations of *p*-nitrophenyl-*β*-D-glucopyranoside and *p*-nitrophenyl-*β*-D-galactopyranoside (0–10 mM) in PBS buffer, pH 7 at 37 °C. Assays were carried out in triplicate (n = 3). The steady-state kinetics parameters (k_{cat} and K_m) were measured by fitting the data to the Michaelis–Menten equation using GraphPad Prism (version 10.1.1) software.

Bacterial strains, cell lines, and growth conditions

The *K. pneumoniae* strains used in this study are KP 529 (hypermucoviscous *K. pneumoniae*), KP 20275, KP 5957, and KP 6070 isolated from clinical samples (Supplementary Table 2) submitted in the Urology and ICU departments of Sir Sunderlal Hospital, Institute of Medical Sciences, Banaras Hindu University, Varanasi, India.

For biofilm formation in vitro, bacteria were grown overnight on Brain Heart Infusion (BHI) agar and then grown in BHI broth for 18 h, and a 1/100 dilution of an overnight culture was used for inoculation. The culture was grown statically for 3 days at 37 °C. To study *K. pneumoniae* growth curves, strains were grown overnight in a BHI medium at 37 °C with shaking. The next day, the cultures were diluted in BHI to absorbance at 600 nm to 0.1, and 1 mL was added to the wells of 24-well plates and grown at 37 °C with shaking in a BioTek Synergy H1 microplate reader. Cell growth was measured as an increase in OD_{600}, with values recorded every 30 min up to 24 h.

The human cell line HeLa cells and murine macrophage (RAW264.7) cells were cultured in Dulbecco's modified Eagle's medium supplemented with 10% fetal bovine serum. THP-1 monocyte cells were cultured in RPMI-1640 glutamax (Sigma) with 10% FBS (Gibco) supplementation and 1% Pen–Strep (Sigma).

Whole genome sequencing and bioinformatic analysis of *Klebsiella pneumoniae* isolates

The overnight grown cultures were pelleted down by centrifugation for 5 min at 12,000 × *g* and subjected to genomic DNA extraction using the QIAamp® DNA Stool Mini Kit (Qiagen) according to the manufacturer's instructions. DNA quality was evaluated using a nanodrop spectrophotometer (Thermo Scientific).

The genome sequencing and the data analysis were carried out by miBiome Therapeutics, India. The libraries were constructed in alignment with whole genome sequencing recommendations of the QIAseq® FX DNA library kit from Qiagen. Briefly, 150 ng of DNA was subjected to fragmentation, end repair, and adapter ligation. Followed by excess adapters were removed using AMPure XP purification beads and the PCR enrichment of adapter-ligated DNA was performed. The resulting library products were cleaned up and were quantitated using a Qubit® fluorometer. Next, the samples were loaded on an HS D1000 screen tape to determine the size range of the fragments and the average library size and subsequently, the libraries were taken ahead for sequencing using Illumina NextSeq 2000. The quality of the raw reads was evaluated using FastQC[67] and the fastp[68] was used to trim and filter the raw reads. The adapters were removed, and the reads were excluded if the average quality of the bases was below 30 over a minimum read length of 50. Reads were re-checked for improvement in quality before moving further ahead. De-novo assembly of cleaned reads was performed using Shovill[69], which has Spades[70] at its core, along with some pre- and post-assembly steps to improve the overall assembly. The

de-novo assembly was performed to generate the genome without biasing the assembly to any characterized genome. The quality of the resulting assembly was then checked with QUAST[71]. To assess the genome completeness and contamination, the CheckM[72] tool was used, which has a predefined and expected set of single-copy marker genes as a proxy for genome-wide completeness. The assembled genome was used for annotation using Bakta v1.9.3[73] with its latest full database version, 5.1. MLST analysis was carried out by MLST tool[74] using PubMLST typing schemes. The complete genotyping, serotyping, and clonal typing were done by Kleborate and Kaptive tool[75].

Inhibition of biofilm formation and biofilm dispersion studies using crystal violet assay

For the biofilm inhibition studies, GH-B2 was added into the growth media while inoculating the bacteria for biofilm formation. At particular time points, the supernatant was decanted and washed once with PBS buffer (pipetting off the supernatant without disturbing the samples), followed by staining with 0.1% crystal violet (CV) for 30 min at room temperature (25 °C). The excess stain was washed with water, and the plates were kept for drying. The residual CV stain was dissolved in an ethanol:acetone (80:20) mixture and absorbance was recorded at 590 nm. For biofilm dispersion studies, the CV staining was performed after treatment of GH-B2 on 3-day-old, pre-formed biofilm. EC_{50} and IC_{50} values were calculated using non-linear least-squares fitting to a dose-response model in Prism 10 software.

Hypermucoviscosity analysis

Hypermucoviscosity was analyzed via string test using a reported protocol[1]. Briefly, all four *K. pneumoniae* isolates were streaked on a MacConkey agar plate and incubated at 37 °C overnight. A colony was lifted using a sterile inoculation loop, and the length of the string from the colony to the loop was measured. A positive string test was defined as viscous strings greater than 5 mm in length. Additionally, sedimentation assays were performed using the reported protocol[1] to validate the hypermucoviscosity quantitatively. All four KP isolates were cultured in BHI media at 37 °C, 180 rpm, for 18 h. The overnight grown culture's optical density at 600 nm (OD_{600}) was adjusted to 1, and 1.5 mL of culture was centrifuged at 2000 × *g* for 5 min. The supernatant was transferred to the 96-well plate without disturbing the pellet, and OD_{600} was measured.

Biofilm matrix isolation

The exopolysaccharides (EPS) from KP biofilm were isolated using a previously reported protocol[76]. Briefly, a 3-day-old mature biofilm of hypermucoviscous *Klebsiella pneumoniae* (KP 529) grown in BHI broth was agitated to isolate the matrix. A 60 µL of formaldehyde (36.5% solution) was added to 10 mL of the dislodged biofilm sludge to fix the cells. The mixture of formaldehyde and biofilm was incubated for 1 h at 25 °C with gentle shaking (100 rpm). The mixture was subsequently incubated for another 3 h after adding 4 mL of 1 M NaOH to each 10 mL of the extract. The resulting suspension was centrifuged at 12,000 × *g* for 1 h at 4 °C. The supernatant containing EPS was dialyzed against distilled water using a 12 KDa molecular weight cut-off membrane for 24 h at 4 °C. Further, the proteins and eDNA were removed by trichloroacetic acid (20% w/v) precipitation, leaving the exopolysaccharides in the extract. Then, 1.5 volumes of cold ethanol were added to the supernatant and kept at −20 °C overnight to separate EPS from lipids. After incubation, the suspension was centrifuged at 12,000 × *g* for 1 h at 4 °C, and the EPS pellet was resuspended in Milli-Q water and dialyzed against Milli-Q water using a 12 KDa molecular weight cut-off membrane for 24 h at 4 °C. The dialyzed EPS was lyophilized overnight and used for further analysis.

Quantitative analysis of hydrolase activity of GH-B2 on *K. pneumoniae* biofilm matrix

The isolated EPS was incubated with GH-B2 overnight with gentle shaking (80 rpm) at 37 °C, followed by quenching by heating at 100 °C for 5 min. Further, the samples were lyophilized and converted to trimethylsilyl derivatives for GC–MS analysis. Briefly, 40 µL of methoxyamine hydrochloride (20 mg in 1 ml pyridine) was added to 2 mg of lyophilized sample and incubated at 65 °C for 1 h. To the incubated solution, 80 µL of BSTFA [*N*,*O*-bis(trimethylsilyl)trifluoro acetamide] + TMCS [trimethylchlorosilane] (99:1 ratio) was added and kept for 1 h incubation at 65 °C. Samples were then diluted with ethyl acetate and injected into GC–MS (Agilent, 8890 GC coupled with the 5977B inert plus MSD) equipped with a HP-5MS UI column (Restek, 30 m x 0.25 mm × 0.25 µm, catalog no. 19091S433UI). The flow rate of the helium carrier gas was maintained at 1.2 mL/min, and the inlet temperature was maintained at 250 °C. A 0.5 µL sample was injected into the system using the autosampler (Agilent, ALS-G4513A) in the split mode with a split ratio of 1:1 and a total flow of 5.4 mL/min. The interface temperature was maintained at 250 °C. The oven temperature was held at 80 °C for 2 min, increased to 170 °C at 15 °C/min, and held for 5 min, then increased to 300 °C at 30 °C/min, at which it was held for 2 min. The mass range for acquiring the data was set at 30–600 m/z. The signal of the silylated glucose *O*-methyl oxime was identified and analyzed using the in-built analysis software (OpenLab CDS, Agilent, version 2.6).

After confirming the release of glucose upon incubation of EPS with GH-B2, further quantification was performed using a spectroscopic method, phenol–sulfuric acid method[77,78]. Briefly, 0.6 mg/mL (10 µM) of GH-B2 was incubated with the extracted exopolysaccharides in PBS buffer, pH 7 at 37 °C. Aliquots were collected at different time intervals, and the samples were heated at 100 °C for 5 min to quench the reaction. A 20 µL sample was mixed with 20 µl 5% phenol. Subsequently, 100 µL sulfuric acid (98%) was added to the mixture and incubated at 25 °C for 10 min. The absorbance of the solution was recorded at 492 nm using the microplate reader. The amount of sugar released was calculated using the calibration curve generated using various known glucose concentrations.

Analysis of the effect of GH-B2 on *K. pneumoniae* cells

To study *K. pneumoniae* growth curves, strains were grown overnight in Brain Heart infusion Broth (BHI) media at 37 °C with shaking. The next day, the cultures were diluted in fresh BHI to absorbance at 600 nm to 0.1, and 1 mL of the culture was added to the well of a 24-well plate and grown at 37 °C with shaking in a BioTek Synergy H1 microplate reader. Cell growth was measured following the increase in OD_{600}, with values recorded every 30 min up to 24 h. The number of viable cells in control and enzyme-treated samples was quantified by CFU analysis. Further, to check any surface alteration induced by GH-B2, the overnight grown KP culture was sub-cultured in fresh BHI media (1:100 dilution) along with GH-B2 (0.3 mg/mL, 5 µM and 0.6 mg/mL, 10 µM), and incubated at 37 °C, with 180 rpm shaking. After 6 h, the OD_{600} was adjusted to the same for all cultures, the cells were pelleted down, and the enzyme was removed by repeated 3-cycles of PBS wash (resuspending gently in 1X PBS and pelleting down the cells) and subjected to analysis. The morphological change of the cells was analyzed by scanning electron microscopy. The samples were further analyzed by zeta potential measurement to check any change in the enzyme-treated cells' surface charge. Briefly, various dilutions (OD_{600}: 0.1, 0.2, and 0.3) of GH-B2-treated cells were prepared in 1X PBS, and the zeta potential was measured using dynamic light scattering spectrometer (Malvern Instruments Limited, UK, Model number: ZEN3600) using zetasizer software with default settings. Further, the cells were subjected to biofilm formation, and the amount of biomass was monitored over a period of 3 days.

Confocal laser scanning microscopy (CLSM) studies

For confocal analysis of enzymatic biofilm dispersion, *K. pneumoniae* biofilm was grown in chambered slides as described before, followed by treatment of the biofilm with GH-B2 (0.3 mg/mL) for 2 h at 37 °C. The residual broth was aspirated, followed by washing thrice with PBS buffer to remove the planktonic cells (pipetting off the supernatant without disturbing the samples). The biofilm was fixed with 3.5% (w/v) paraformaldehyde for 30 min at room temperature. A 50 µL solution of Texas red conjugated with Concanavalin A (1 mg/mL) was applied directly to the top of the biofilm, and the sample was kept in the dark for 30 min. The

representative images were taken using the Zeiss LSM 880 multi-photon inverted confocal laser-scanning microscope (Carl Zeiss, Jena, Germany). Images were obtained via a plan-apochromat 63X/1.4 oil DIC M27 objective with a z-step of 0.45 µm. Images were processed using the ZenBlack software.

For the mean fluorescence intensity (MFI) calculation, 10 images per sample were acquired using Zeiss LSM 710 (Carl Zeiss, Jena, Germany) via a plan-apochromat 63X/1.4 oil DIC M27 objective with a z-step of 1 µm. The MFI was normalized to the intensity of the bright field of the same image. Concanavalin-tagged Texas red (548–690 nm), Alexa fluor 488 (487–572 nm), propidium iodide (581–719 nm), and Syto 9 (495–520 nm) were the laser channels employed for the study.

Scanning electron microscopy (SEM) studies

Round microscopic cover glass (12 mm, Blue Star) and the latex Foley catheter (4 mm diameter, latex Foley balloon catheter, Teleflex) 1 cm pieces, Teleflex Medical Private Ltd., India were sterilized by autoclaving and placed in a 24-well plate, which was followed by inoculation of *K. pneumoniae*. The biofilm was grown in the microtiter plate as described above. Afterward, under static conditions, GH-B2 (0.3 mg/mL) treatment was carried out for 2 h at 37 °C. The treated biofilm samples were chemically fixed using 2.5% glutaraldehyde and incubated overnight at 4 °C. Subsequently, the coverslips were washed with Milli-Q water to remove the traces of glutaraldehyde, followed by dehydration of samples using a gradient of ethanol (30, 50, 75, 85, 95, and 100% v/v) for 3 min each (pipetting off the supernatant without disturbing the samples). Before imaging, the samples were coated with gold using BAL-TEC SCD 500 sputter coater (Thermo Fisher Scientific). The images were acquired using JSM-IT300 InTouchScope™ Scanning Electron Microscope with a high probe current of 30 nA, acceleration voltage of 15 KV, and working distance of ~12 mm.

The thickness of the biofilm was analyzed by placing the samples (glass coverslip/ catheter) on a vertical stub (double 90 SEM pin stub of diameter 12.7 mm) for imaging. Subsequently, the thickness of the biofilm was measured from the acquired images using JEOL software.

Viable cell (CFU) analysis to quantify enzymatic dispersion of biofilm

Three-day-old biofilms were grown on a glass coverslip and Foley catheter. The media was removed and washed thrice with 1X PBS to remove the unattached cells, which was followed by treatment with 1 mL of PBS along with GH-B2 (5 µM, 0.3 mg/mL) and incubation at 37 °C. After 2 h, the supernatant was collected to quantify the enzymatically dispersed cells. Followed by the glass coverslip and Foley catheter were washed once with PBS to remove unattached cells (pipetting off the supernatant without disturbing the samples). Again, 1 mL of PBS was added to the coverslip and was scraped to remove the remaining biofilm adhered to the coverslip. The catheter piece was transferred to 1 mL PBS in a tube and vortexed to extract the remaining biofilm on the catheter. The samples were serially diluted and plated on differential cystine–lactose–electrolyte-deficient (C.L.E.D) agar. The plates were incubated at 37 °C and the colonies were counted after 24 h and reported as $\log_{10}$ CFU.mL^{-1} for glass coverslip samples and $\log_{10}$ CFU gm^{-1} mL^{-1} for catheter samples.

Evaluating antibiotic sensitivity to *K. pneumoniae*

The minimum inhibitory concentration (MIC, the lowest concentration of antibiotic at which no obvious growth of microorganism was observed) of meropenem was calculated using the broth microdilution method. The planktonic MIC was established using guidelines of European Committee on Antimicrobial Susceptibility Testing (EUCAST) criteria[79,80]. Briefly, the 96-well microtiter plates having serially diluted antibiotic (from 2 to 0.0002 mg mL^{-1}) in sterile Mueller-Hinton broth were inoculated with *K. pneumoniae* culture at the final inoculum density of 10^5 CFU mL^{-1} per well. The 96-well microtiter plates were incubated at 37 °C for 24 h with 180 rpm shaking. The MICs were noted as the minimal amounts of antibiotic at which no visible growth was observed in the microtiter plate wells. The sterile broth served as a control. The MIC of the antibiotic was determined using the absorbance at 600 nm. All the experiments were performed in triplicate ($n = 3$).

MBEC (minimum biofilm eradication concentration) was determined by adding the serially diluted antibiotic to 3-day-old biofilms and incubating at 37 °C for 18 h with 180 rpm shaking[81]. Non-adherent cells were gently washed out of the mature biofilms with MHI broth before adding the antibiotics. To investigate whether GH-B2 can improve the susceptibility of biofilm-encased *K. pneumoniae* cells to antibiotics, we tested the MBECs of meropenem against GH-B2-dispersed bacteria from 3-day-old biofilms. Briefly, serially diluted antibiotics and GH-B2 were added to 3-day-old biofilms and incubated at 37 °C for 18 h with 180 rpm shaking. Cell viability was calculated using the following formula: cell viability (%) = ((mean signal of corresponding well − mean signal of negative control well)/(mean signal of positive control well − mean signal of negative control well)) × 100. All experiments were performed in triplicate ($n = 3$) and repeated three times.

Experimental evolution of *Klebsiella pneumoniae* against meropenem

The overnight grown *K. pneumoniae* culture (G0) was subjected to biofilm formation (1/100 dilution in BHI media) in a 24-well plate. After 3 days of biofilm formation, the supernatant was removed, and fresh BHI media was added along with meropenem (16 µg/mL) in one group and meropenem (16 µg/mL) with GH-B2 (5 µM, 0.3 mg/mL) in another group and incubated at 37 °C, 180 rpm shaking for 18 h. The evolved populations (G1) were stored as glycerol stock at −80 °C and parallelly subjected to biofilm formation (10 µL in 1 mL BHI media). After 3 days of biofilm formation, the procedure was repeated for 3 more cycles (Supplementary Fig. 13a). At the endpoint of the experiment, all the glycerol stocks were revived and subjected to MIC (minimum inhibitory concentration) testing (detailed procedure of MIC analysis mentioned above).

Determination of the synergistic effect of GH-B2 with antibiotic

The minimum inhibitory concentration (MIC, the lowest concentration of antibiotic required for preventing the growth of a planktonic bacterial population) and minimum biofilm eradication concentration (MBEC, lowest antibiotic concentration that inhibits re-growth of bacteria from the treated biofilms) of meropenem were calculated using the broth microdilution method, as reported previously[79–81]. The potentiation of meropenem by GH-B2 against biofilm-encased *K. pneumoniae* was determined using CFU analysis and CLSM studies. Biofilm was treated with GH-B2 (0.3 mg/mL) for 2 h at 37 °C followed by meropenem (250 µg/mL) for 24 h at 37 °C, and the viability of cells was monitored employing the LIVE/DEAD cell imaging kit according to the manufacturer's instructions followed by CLSM imaging as described previously. The LIVE/DEAD assay involves Syto 9 (with excitation and emission maxima at 480 nm and 500 nm, respectively), which stains (green) the nucleic acids of both the live and dead cells and propidium iodide (PI) (with excitation and emission maxima at 490 and 635 nm, respectively), which only stains (red) the DNA of cells with damaged membrane. Although Syto 9 stains dead cells, PI has a higher affinity for DNA, displacing Syto 9 from the dead cell's nucleic acids[82].

Phagocytosis assay

K. pneumoniae biofilm was grown on sterile glass coverslips in BHI broth at 37 °C for 3 days. The biofilm was treated with GH-B2 (0.3 mg/mL) at 37 °C for 2 h. The supernatant was removed and washed with 1X PBS before incubating with RAW264.7 macrophage cells (5×10^5) in Dulbecco's modified Eagle medium (DMEM) media (supplemented with 10% fetal bovine serum) at 37 °C, in the presence of 5% CO_2 for 2 h. The supernatant was removed, and samples were washed with PBS buffer and processed for SEM imaging and CLSM studies. Also, the remaining biofilm was scraped off the glass coverslips, resuspended in 1 mL of PBS buffer, and analyzed by CFU determination. THP-1 cells were cultured in RPMI-1640 glutamax with 10% FBS supplementation and 1% Pen–Strep. The cells were washed with 1X PBS prior to seeding onto the biofilm-containing 24-well plates.

5×10^5 cells were seeded on the biofilm-containing plate in RPMI-1640 glutamax with 10% FBS and supplemented with PMA (phorbol 12-myristate-13-acetate at a final concentration of 25 ng/mL) for activation of the monocytes. The plate was incubated at 37 °C in a humidified incubator with 5% CO_2 for 20 h. The supernatant was removed, and samples were washed with PBS buffer and processed for SEM imaging and CLSM studies. For CFU analysis, the cells adhered to the surface were collected by scraping the biofilm from the coverslip using 1 mL of 1X PBS. Further, the biofilm suspension was plated on C.L.E.D agar to determine the CFU. Experiments were performed in three replicates ($n = 3$).

For confocal imaging, the samples were fixed with 3.5% paraformaldehyde (w/v) for 30 min at room temperature (25 °C), followed by one wash with 1X PBS and treatment with *K. pneumoniae* polyclonal antibody. The antibody was used at a dilution of 1:200 in the blocking buffer (2% BSA and 0.01% saponin). The samples were incubated at 4 °C overnight in a wet chamber, washed with 1X PBS, and stained with the secondary antibody (anti-Rabbit Alexa fluor 488, 1:200 dilution in the same blocking buffer). The samples were incubated at room temperature for 1 h, washed with 1X PBS, and stained with propidium iodide. After 30 min of incubation at room temperature, samples were again washed once with 1X PBS and mounted to the glass slide, and images were acquired.

Cytotoxicity analysis

HeLa cells were used for cytotoxicity analysis of GH-B2. Cells were cultured in DMEM media supplemented with 10% FBS at 37 °C in the presence of 5% CO_2. The cells were seeded (10,000 cells/well) in 96-well tissue culture plates and incubated overnight. The media was replaced with enzyme (0.3 and 0.6 mg/mL of GH-B2) in fresh culture media, and cytotoxicity was monitored at 2 and 12 h intervals. After the incubation with the enzyme, 3-(4,5-dimethylthiazol-2-yl)-2,5-diphenyltetrazolium bromide (MTT, 0.5 mg/mL) was added to the suspension and incubated for 3 h at 37 °C. The culture medium was subsequently removed, and the formazan crystals were solubilized using 100 µL DMSO. The absorbance of the solution was measured after 15 min at 570 nm using the BioTek Synergy H1 microplate reader. Cell viability was expressed as a percentage relative to untreated cells. Experiments were performed in triplicate ($n = 3$).

Chronic wound infection model study in mice

Twelve-to-fourteen-week-old BALB/C mice were used to create the murine chronic wound infection model[83]. Mice were anesthetized with an intraperitoneal injection of xylazine (4.5 mg/kg body weight of mice) and ketamine (90 mg/kg body weight of mice). The 8 mm diameter circular wounds were created on the back of anesthetized mice using a sterile biopsy punch, followed by fixing 0.5 mm thick ring-shaped silicone splints with 8 mm inner diameter to the surrounding wound edge using an instant bonding cyano-acrylate adhesive (glue). Thus, silicon rings tightly adhere to the skin around the wound, preventing local skin contraction. Further, the wounds were covered with a semipermeable polyurethane dressing under which *K. pneumoniae* cells (10^{10}) were injected into the wound bed, which was further covered with an elastic bandage. Biofilm formation was allowed to proceed for 3 days. Four groups of mice were created; one group was treated with PBS buffer control, the second group was treated with meropenem, the third group was treated with GH-B2 (0.6 mg/mL in 100 µL solution/wound), and the fourth group was treated with both GH-B2 (0.6 mg/mL in 100 µL solution/wound) and meropenem (512 µg in 100 µL solutions/wound) for 4 days. The treatments were done once a day via direct topical injection using a syringe, and the wounds were photographed to check the healing. To study the colonization in organs, tissues from the right and left lungs, mesenteric lymph nodes, and spleen were isolated aseptically (in biosafety level 2 cabinet) 7 days post-infection (4 days post-treatment). To study systemic dissemination, blood was isolated by cardiac puncture prior to the isolation of tissue from organs, and an anticoagulant (3.25% tri-sodium citrate) was used to prevent coagulation. The tissues were homogenized using glass lysis beads (1 mm, BioSpec) using a bead-beater (BioSpec). The lysate and blood were used for CFU analysis on differential and selective C.L.E.D agar by serial dilution. The wound beds were harvested for CFU and histopathology analysis. The wound tissue was collected and fixed in 10% neutral buffered formalin for histopathology. The fixed tissues were embedded in paraffin, cut into a 4 µm section by microtome, and mounted on glass slides. The wound tissue sections were stained with hematoxylin and eosin (H&E) for histopathological analysis and photography.

Statistical analysis

All the graphs reported in this study were plotted using GraphPad Prism software (version 10.1.1). The statistical analysis was performed using one-way ANOVA with Dunnet's post-hoc test or two-way ANOVA with Tukey's post-hoc test. The data represents the mean ± standard deviation. The number of replicates and the significantly different results are designated with a graphic feature '*', and the non-significant results are designated with 'ns' within the corresponding figures.

Data availability

The phylogenetic tree is available in Interactive Tree of Life (iTOL, https://itol.embl.de/tree/14139128121521216865701 71). The genome sequencing data of four clinical *Klebsiella pneumoniae* isolates used in this study have been deposited in the NCBI database under the Bioproject ID PRJNA1171173. The source data corresponding to Figs. 1–7 are provided as a source data file. Any additional data are available from the corresponding authors upon reasonable request.

Received: 9 April 2024; Accepted: 21 October 2024;
Published online: 05 November 2024

References

1. Kochan, T. J. et al. *Klebsiella pneumoniae* clinical isolates with features of both multidrug-resistance and hypervirulence have unexpectedly low virulence. *Nat. Commun.* **14**, 7962 (2023).
2. Verani, J. R. et al. Child deaths caused by *Klebsiella pneumoniae* in sub-Saharan Africa and South Asia: a secondary analysis of Child Health and Mortality Prevention Surveillance (CHAMPS) data. *Lancet Microbe* **5**, e131–e141 (2024).
3. Cillóniz, C., Dominedò, C. & Torres, A. Multidrug resistant gram-negative bacteria in community-acquired pneumonia. *Crit. Care* **34**, 459–475 (2019).
4. David, S. et al. Epidemic of carbapenem-resistant *Klebsiella pneumoniae* in Europe is driven by nosocomial spread. *Nat. Microbiol.* **4**, 1919–1929 (2019).
5. Munoz-Price, L. S. et al. Clinical epidemiology of the global expansion of *Klebsiella pneumoniae* carbapenemases. *Lancet Infect. Dis.* **13**, 785–796 (2013).
6. Rathore, S. S., Cheepurupalli, L., Gangwar, J., Raman, T. & Ramakrishnan, J. Biofilm of *Klebsiella pneumoniae* minimize phagocytosis and cytokine expression by macrophage cell line. *AMB Express* **12**, 122 (2022).
7. Penesyan, A., Nagy, S. S., Kjelleberg, S., Gillings, M. R. & Paulsen, I. T. Rapid microevolution of biofilm cells in response to antibiotics. *npj Biofilms Microbiomes* **5**, 34 (2019).
8. Walker, K. A. & Miller, V. L. The intersection of capsule gene expression, hypermucoviscosity and hypervirulence in *Klebsiella pneumoniae*. *Curr. Opin. Microbiol.* **54**, 95–102 (2020).
9. Shon, A. S., Bajwa, R. P. & Russo, T. A. Hypervirulent (hypermucoviscous) *Klebsiella pneumoniae*: a new and dangerous breed. *Virulence* **4**, 107–118 (2013).
10. Mike, L. A. et al. A systematic analysis of hypermucoviscosity and capsule reveals distinct and overlapping genes that impact *Klebsiella pneumoniae* fitness. *PLoS Pathog.* **17**, e1009376 (2021).
11. Vandhana, V., Saralaya, K. V., Bhat, S., Shenoy Mulki, S. & Bhat, A. K. Characterization of hypervirulent *Klebsiella pneumoniae* (Hv-Kp): correlation of virulence with antimicrobial susceptibility. *Int. J. Microbiol.* **2022**, 4532707 (2022).

12. Murray, C. J. et al. Global burden of bacterial antimicrobial resistance in 2019: a systematic analysis. *Lancet* **399**, 629–655 (2022).
13. Karygianni, L., Ren, Z., Koo, H. & Thurnheer, T. Biofilm matrixome: extracellular components in structured microbial communities. *Trends Microbiol.* **28**, 668–681 (2020).
14. Redman, W. K. et al. Efficacy and safety of biofilm dispersal by glycoside hydrolases in wounds. *Biofilm* **3**, 100061 (2021).
15. Yu, S. et al. PslG, a self-produced glycosyl hydrolase, triggers biofilm disassembly by disrupting exopolysaccharide matrix. *Cell Res.* **25**, 1352–1367 (2015).
16. Ramakrishnan, R., Singh, A. K., Singh, S., Chakravortty, D. & Das, D. Enzymatic dispersion of biofilms: an emerging biocatalytic avenue to combat biofilm-mediated microbial infections. *J. Biol. Chem.* **298**, 102352 (2022).
17. Fleming, D. & Rumbaugh, K. P. Approaches to dispersing medical biofilms. *Microorganisms* **5**, 15 (2017).
18. Wang, S. et al. Strategy to combat biofilms: a focus on biofilm dispersal enzymes. *npj Biofilms Microbiomes* **9**, 63 (2023).
19. Hess, M. et al. Metagenomic discovery of biomass-degrading genes and genomes from cow rumen. *Science* **331**, 463–467 (2011).
20. Del Pozo, M. V. et al. Microbial β-glucosidases from cow rumen metagenome enhance the saccharification of lignocellulose in combination with commercial cellulase cocktail. *Biotechnol. Biofuels* **5**, 1–13 (2012).
21. Gharechahi, J. et al. Lignocellulose degradation by rumen bacterial communities: new insights from metagenome analyses. *Environ. Res.* **229**, 115925 (2023).
22. Mello, L. V., Chen, X. & Rigden, D. J. Mining metagenomic data for novel domains: BACON, a new carbohydrate-binding module. *FEBS Lett.* **584**, 2421–2426 (2010).
23. Varadi, M. et al. AlphaFold protein structure database: massively expanding the structural coverage of protein-sequence space with high-accuracy models. *Nucleic Acids Res.* **50**, D439–D444 (2021).
24. York, A. Naturally modified cellulose in bacterial biofilms. *Nat. Rev. Microbiol.* **16**, 123–123 (2018).
25. Heredia-Ponce, Z. et al. Biological role of EPS from *Pseudomonas syringae* pv. syringae UMAF0158 extracellular matrix, focusing on a Psl-like polysaccharide. *npj Biofilms Microbiomes* **6**, 37 (2020).
26. Yang, Y. et al. A mechanism of glucose tolerance and stimulation of GH1 β-glucosidases. *Sci. Rep.* **5**, 1–12 (2015).
27. Howell, J. & Stuck, J. Kinetics of solka floc cellulose hydrolysis by *Trichoderma viride* cellulase. *Biotechnol. Bioeng.* **17**, 873–893 (1975).
28. Fang, C.-T., Chuang, Y.-P., Shun, C.-T., Chang, S.-C. & Wang, J.-T. A novel virulence gene in *Klebsiella pneumoniae* strains causing primary liver abscess and septic metastatic complications. *J. Exp. Med.* **199**, 697–705 (2004).
29. Lee, C.-R. et al. Antimicrobial resistance of hypervirulent *Klebsiella pneumoniae*: epidemiology, hypervirulence-associated determinants, and resistance mechanisms. *Front. Cell. Infect. Microbiol.* **7**, 483 (2017).
30. De los Santos, L. et al. Polyproline peptide targets *Klebsiella pneumoniae* polysaccharides to collapse biofilms. *Cell Rep. Phys. Sci.* **5**, 101869 (2024).
31. Chakraborty, P., Bajeli, S., Kaushal, D., Radotra, B. D. & Kumar, A. Biofilm formation in the lung contributes to virulence and drug tolerance of *Mycobacterium tuberculosis*. *Nat. Commun.* **12**, 1606 (2021).
32. Goldstein, I., Hollerman, C. & Merrick, J. M. Protein-carbohydrate interaction I. The interaction of polysaccharides with concanavalin A. *Biochim. Biophys. Acta.* **97**, 68–76 (1965).
33. Redman, W. K., Welch, G. S. & Rumbaugh, K. P. Differential efficacy of glycoside hydrolases to disperse biofilms. *Front. Cell. Infect. Microbiol.* **10**, 379 (2020).
34. Luo, A., Wang, F., Sun, D., Liu, X. & Xin, B. Formation, development, and cross-species interactions in biofilms. *Front. Microbiol.* **12**, 757327 (2022).
35. Assefa, M. & Amare, A. Biofilm-associated multi-drug resistance in hospital-acquired infections: a review. *Infect. Drug Resist.* **15**, 5061–5068 (2022).
36. Benincasa, M. et al. Biofilms from *Klebsiella pneumoniae*: matrix polysaccharide structure and interactions with antimicrobial peptides. *Microorganisms* **4**, 26 (2016).
37. Li, Y. & Ni, M. Regulation of biofilm formation in *Klebsiella pneumoniae*. *Front. Microbiol.* **14**, 1238482 (2023).
38. Sharma, S. et al. Characterizing and demonstrating the role of *Klebsiella* SSN1 exopolysaccharide in osmotic stress tolerance using neutron radiography. *Sci. Rep.* **13**, 10052 (2023).
39. Feneley, R. C., Hopley, I. B. & Wells, P. N. Urinary catheters: history, current status, adverse events and research agenda. *J. Med. Eng. Technol.* **39**, 459–470 (2015).
40. Lee, K.-H. et al. The influence of urinary catheter materials on forming biofilms of microorganisms. *J. Bacteriol. Virol.* **47**, 32–40 (2017).
41. Tamura, N., Gasparetto, A. & Svidzinski, T. Evaluation of the adherence of *Candida* species to urinary catheters. *Mycopathologia* **156**, 269–272 (2003).
42. Nye, T. M. et al. Microbial co-occurrences on catheters from long-term catheterized patients. *Nat. Commun.* **15**, 61 (2024).
43. Townsend, E. M., Moat, J. & Jameson, E. CAUTI's next top model–Model dependent *Klebsiella* biofilm inhibition by bacteriophages and antimicrobials. *Biofilm* **2**, 100038 (2020).
44. Wu, Y. et al. A novel polysaccharide depolymerase encoded by the phage SH-KP152226 confers specific activity against multidrug-resistant *Klebsiella pneumoniae* via biofilm degradation. *Front. Microbiol.* **10**, 2768 (2019).
45. Fursov, M. V. et al. Antibiofilm activity of a broad-range recombinant endolysin LysECD7: in vitro and in vivo study. *Viruses* **12**, 545 (2020).
46. Blasco, L. et al. In vitro and in vivo efficacy of combinations of colistin and different endolysins against clinical strains of multi-drug resistant pathogens. *Sci. Rep.* **10**, 7163 (2020).
47. Rogers, G. B., Carroll, M. P. & Bruce, K. D. Enhancing the utility of existing antibiotics by targeting bacterial behaviour? *Br. J. Pharmacol.* **165**, 845–857 (2012).
48. Cook, M. A. & Wright, G. D. The past, present, and future of antibiotics. *Sci. Transl. Med.* **14**, eabo7793 (2022).
49. Devanga Ragupathi, N. K. et al. The influence of biofilms on carbapenem susceptibility and patient outcome in device associated *K. pneumoniae* infections: insights into phenotype vs genome-wide analysis and correlation. *Front. Microbiol.* **11**, 591679 (2020).
50. Sawa, T., Kooguchi, K. & Moriyama, K. Molecular diversity of extended-spectrum β-lactamases and carbapenemases, and antimicrobial resistance. *J. Intensive Care* **8**, 13 (2020).
51. Zhou, X.-Y. et al. In vitro characterization and inhibition of the interaction between ciprofloxacin and berberine against multidrug-resistant *Klebsiella pneumoniae*. *J. Antibiot.* **69**, 741–746 (2016).
52. Nordmann, P., Cuzon, G. & Naas, T. The real threat of *Klebsiella pneumoniae* carbapenemase-producing bacteria. *Lancet Infect. Dis.* **9**, 228–236 (2009).
53. Pournaras, S. et al. Characteristics of meropenem heteroresistance in *Klebsiella pneumoniae* carbapenemase (KPC)-producing clinical isolates of *K. pneumoniae*. *J. Clin. Microbiol.* **48**, 2601–2604 (2010).
54. Stewart, P. S. & Costerton, J. W. Antibiotic resistance of bacteria in biofilms. *Lancet* **358**, 135–138 (2001).
55. Ahmed, M. N., Porse, A., Sommer, M. O. A., Høiby, N. & Ciofu, O. Evolution of antibiotic resistance in biofilm and planktonic *Pseudomonas aeruginosa* populations exposed to subinhibitory levels of ciprofloxacin. *Antimicrob. Agents Chemother.* **62**, 00320–00318 (2018).
56. Guilhen, C. et al. Colonization and immune modulation properties of *Klebsiella pneumoniae* biofilm-dispersed cells. *npj Biofilms Microbiomes* **5**, 25 (2019).
57. Liu, S. et al. Assessment of antimicrobial and wound healing effects of Brevinin-2Ta against the bacterium *Klebsiella pneumoniae* in dermally-wounded rats. *Oncotarget* **8**, 111369 (2017).

58. Thompson, M. G. et al. Evaluation of gallium citrate formulations against a multidrug-resistant strain of *Klebsiella pneumoniae* in a murine wound model of infection. *Antimicrob. Agents Chemother.* **59**, 6484–6493 (2015).
59. Madeira, F. et al. The EMBL-EBI search and sequence analysis tools APIs in 2019. *Nucleic Acids Res.* **47**, W636–W641 (2019).
60. Letunic, I. & Bork, P. Interactive tree of life (iTOL) v3: an online tool for the display and annotation of phylogenetic and other trees. *Nucleic Acids Res.* **44**, W242–W245 (2016).
61. Mistry, J. et al. Pfam: The protein families database in 2021. *Nucleic Acids Res.* **49**, D412–D419 (2021).
62. Waterhouse, A. et al. SWISS-MODEL: homology modelling of protein structures and complexes. *Nucleic Acids Res.* **46**, W296–W303 (2018).
63. Iqbal, T. & Das, D. Biochemical investigation of membrane-bound cytochrome b5 and the catalytic domain of cytochrome b5 reductase from *Arabidopsis thaliana*. *Biochemistry* **61**, 909–921 (2022).
64. Miller, G. L. Use of dinitrosalicylic acid reagent for determination of reducing sugar. *Anal. Chem.* **31**, 426–428 (1959).
65. Schwald, W., Chan, M., Breuil, C. & Saddler, J. Comparison of HPLC and colorimetric methods for measuring cellulolytic activity. *Appl. Microbiol. Biotechnol.* **28**, 398–403 (1988).
66. Leadbeater, D. R. & Bruce, N. C. Functional characterisation of a new halotolerant seawater active glycoside hydrolase family 6 cellobiohydrolase from a salt marsh. *Sci. Rep.* **14**, 3205 (2024).
67. Andrews, S. et al. FastQC. *A Quality Control Tool for High Throughput Sequence Data* **370**, https://www.bioinformatics.babraham.ac.uk/projects/fastqc/ (2010).
68. Chen, S., Zhou, Y., Chen, Y. & Gu, J. fastp: an ultra-fast all-in-one FASTQ preprocessor. *Bioinformatics* **34**, i884–i890 (2018).
69. Seemann, T. S. *Faster SPAdes (or Better SKESA/Megahit/Velvet) Assembly of Illumina Reads* https://github.com/tseemann/shovill (2018).
70. Bankevich, A. et al. SPAdes: a new genome assembly algorithm and its applications to single-cell sequencing. *J. Comput. Biol.* **19**, 455–477 (2012).
71. Gurevich, A., Saveliev, V., Vyahhi, N. & Tesler, G. QUAST: quality assessment tool for genome assemblies. *Bioinformatics* **29**, 1072–1075 (2013).
72. Parks, D. H., Imelfort, M., Skennerton, C. T., Hugenholtz, P. & Tyson, G. W. CheckM: assessing the quality of microbial genomes recovered from isolates, single cells, and metagenomes. *Genome Res.* **25**, 1043–1055 (2015).
73. Schwengers, O. et al. Bakta: rapid and standardized annotation of bacterial genomes via alignment-free sequence identification. *Microb. Genom.* **7**, 000685 (2021).
74. Jolley, K. A. & Maiden, M. C. BIGSdb: scalable analysis of bacterial genome variation at the population level. *BMC Bioinform.* **11**, 1–11 (2010).
75. Lam, M. M. et al. A genomic surveillance framework and genotyping tool for *Klebsiella pneumoniae* and its related species complex. *Nat. Commun.* **12**, 4188 (2021).
76. Bales, P. M., Renke, E. M., May, S. L., Shen, Y. & Nelson, D. C. Purification and characterization of biofilm-associated EPS exopolysaccharides from ESKAPE organisms and other pathogens. *PLoS ONE* **8**, e67950 (2013).
77. DuBois, M., Gilles, K. A., Hamilton, J. K., Rebers, P. A. & Smith, F. Colorimetric method for determination of sugars and related substances. *Anal. Chem.* **28**, 350–356 (1956).
78. Singh, A. K. et al. Classification of clinical isolates of *Klebsiella pneumoniae* based on their in vitro biofilm forming capabilities and elucidation of the biofilm matrix chemistry with special reference to the protein content. *Front. Microbiol.* **10**, 669 (2019).
79. EUCAST. *Clinical Breakpoints* (European Committee on Antimicrobial Susceptibility Testing, 2011).
80. Patel, J. B. *Performance Standards for Antimicrobial Susceptibility Testing; Twenty-Fifth Informational Supplement*. (Clinical and Laboratory Standards Institute, Wayne, 2015).
81. Wannigama, D. L. et al. Simple fluorometric-based assay of antibiotic effectiveness for *Acinetobacter baumannii* biofilms. *Sci. Rep.* **9**, 6300 (2019).
82. Warraich, A. A. et al. Evaluation of anti-biofilm activity of acidic amino acids and synergy with ciprofloxacin on *Staphylococcus aureus* biofilms. *Sci. Rep.* **10**, 1–14 (2020).
83. Wang, X., Ge, J., Tredget, E. E. & Wu, Y. The mouse excisional wound splinting model, including applications for stem cell transplantation. *Nat. Protoc.* **8**, 302–309 (2013).

Acknowledgements

D.D. acknowledges the Science and Engineering Research Board (CRG/2023/000760), India, and the Indian Institute of Science (IISc), Bangalore, India, (SR/MHRD-18-0021) for financial support. D.C. acknowledges TATA Innovation Fellowship, DAE-SRC Fellowship, and DBT-IISc IOE for support. R.R. acknowledges the Prime Minister's Research Fellowship, Government of India, for support. The authors thank Prof. Pradyot Prakash (Department of Microbiology, Institute of Medical Sciences, BHU, India) for kindly providing the clinical isolates of *Klebsiella pneumoniae* and methicillin-resistant *Staphylococcus aureus* (MRSA). The authors thank Prof. Anne Blanc-Pottard (Laboratory of Pathogens and Host Immunity, Université Montpellier, France) for kindly providing the *Pseudomonas aeruginosa* (PAO1) strain. The authors thank Prof. Nagasuma Chandra (Department of Biochemistry, IISc Bangalore, India) for kindly providing the *Enterobacter aerogenes* (EA) strain. We thank miBiome Therapeutics, India, for conducting the genomic sequencing and bioinformatic analyses.

Author contributions

D.D., D.C., and R.R. conceived the project and designed the experiments. R.R. carried out the enzyme expression, purification, and biochemical characterization. R.R., A.V.N., and K.P. performed the in vitro biofilm dispersion studies and R.S.R. performed the in vivo studies. R.R., A.V.N., K.P., R.S.R., D.C, and D.D. analyzed the data. R.R., D.C., and D.D. wrote the manuscript. All authors discussed the results, reviewed, and edited the manuscript.

Competing interests

The authors declare a conflict of interest in the work and filed a patent application to protect the findings. Applicant: Indian Institute of Science, Bangalore, India. Name of inventors: D.D., D.C., R.R., A.V.N., and K.P. Application No. 202341053814, which has been granted (Indian Patent No. 524536).

Ethics approval

The animal study was reviewed and approved by the IAEC (Institutional Animal Ethical Committee) of the Indian Institute of Science, Bangalore, India (Approval Issue No.: CAF/ETHICS/953/2023).

Additional information

Supplementary information The online version contains supplementary material available at https://doi.org/10.1038/s41522-024-00593-7.

Correspondence and requests for materials should be addressed to Dipshikha Chakravortty or Debasis Das.